Monthly Notices
of the
ROYAL ASTRONOMICAL SOCIETY

Mon. Not. R. Astron. Soc. **404,** 1639–1671 (2010) doi:10.1111/j.1365-2966.2010.16407.x

Evolutionary stellar population synthesis with MILES – I. The base models and a new line index system

A. Vazdekis,[1,2]★ P. Sánchez-Blázquez,[1,2] J. Falcón-Barroso,[1,2] A. J. Cenarro,[1,2,3] M. A. Beasley[1] N. Cardiel,[4] J. Gorgas[4] and R. F. Peletier[5]

[1]*Instituto de Astrofísica de Canarias, La Laguna, E-38200 Tenerife, Spain*
[2]*Departamento de Astrofísica, Universidad de La Laguna, E-38205 La Laguna, Tenerife, Spain*
[3]*Centro de Estudios de Física del Cosmos de Aragón, C/ General Pizarro 1, E-44001 Teruel, Spain*
[4]*Departamento de Astrofísica, Facultad de Ciencias Físicas, Universidad Complutense de Madrid, E-28040 Madrid, Spain*
[5]*Kapteyn Astronomical Institute, University of Groningen, Postbus 800, 9700 AV, Groningen, the Netherlands*

Accepted 2010 January 22. Received 2010 January 22; in original form 2009 August 3

ABSTRACT

We present synthetic spectral energy distributions (SEDs) for single-age, single-metallicity stellar populations (SSPs) covering the full optical spectral range at moderately high resolution [full width at half-maximum (FWHM) = 2.3 Å]. These SEDs constitute our base models, as they combine scaled-solar isochrones with an empirical stellar spectral library [Medium resolution INT Library of Empirical Spectra (MILES)], which follows the chemical evolution pattern of the solar neighbourhood. The models rely as much as possible on empirical ingredients, not just on the stellar spectra, but also on extensive photometric libraries, which are used to determine the transformations from the theoretical parameters of the isochrones to observational quantities. The unprecedented stellar parameter coverage of the MILES stellar library allowed us to safely extend our optical SSP SED predictions from intermediate- to very-old-age regimes and the metallicity coverage of the SSPs from super-solar to [M/H] = −2.3. SSPs with such low metallicities are particularly useful for globular cluster studies. We have computed SSP SEDs for a suite of initial mass function shapes and slopes. We provide a quantitative analysis of the dependence of the synthesized SSP SEDs on the (in)complete coverage of the stellar parameter space in the input library that not only shows that our models are of higher quality than those of other works, but also in which range of SSP parameters our models are reliable. The SSP SEDs are a useful tool to perform the analysis of stellar populations in a very flexible manner. Observed spectra can be studied by means of full spectrum fitting or by using line indices. For the latter, we propose a new line index system to avoid the intrinsic uncertainties associated with the popular Lick/IDS system and provide more appropriate, uniform, spectral resolution. Apart from constant resolution as a function of wavelength, the system is also based on flux-calibrated spectra. Data can be analysed at three different resolutions: 5, 8.4 and 14 Å (FWHM), which are appropriate for studying globular cluster, low- and intermediate-mass galaxies, and massive galaxies, respectively. Furthermore, we provide polynomials to transform current Lick/IDS line index measurements to the new system. We provide line index tables in the new system for various popular samples of Galactic globular clusters and galaxies. We apply the models to various stellar clusters and galaxies with high-quality spectra, for which independent studies are available, obtaining excellent results. Finally, we designed a web page from which not only these models and stellar libraries can be downloaded but which also provides a suite of on-line tools to facilitate the handling and transformation of the spectra.

Key words: globular clusters: general – galaxies: abundances – galaxies: elliptical and lenticular, cD – galaxies: stellar content.

★E-mail: vazdekis@iac.es

1 INTRODUCTION

To obtain information about unresolved stellar populations in galaxies, one can look at colours, ranging from the ultraviolet (UV) to the infrared (IR). Such a method is popular especially when studying faint objects. Since colours are strongly affected by dust extinction, one prefers to use spectra when studying brighter objects. These have the additional advantage that abundances of various elements can be studied, from the strength of absorption lines (e.g. Rose 1985; Sánchez-Blázquez et al. 2003; Carretero et al. 2004). Although the UV and the near-IR are promising wavelength regions to study, the large majority of spectral studies is done in the optical, mainly because of our better understanding of the region. To obtain information, one generally compares model predictions with measurements of strong absorption-line strengths. This method, which is insensitive to the effects of dust extinction (e.g. MacArthur 2005), very often uses the Lick/IDS system of indices, which comprises definitions of 25 absorption-line strengths in the optical spectral range, originally defined on a low-resolution stellar library [full width at half-maximum (FWHM) > 8–11 Å; Gorgas et al. 1993; Worthey et al. 1994; Worthey & Ottaviani 1997]. There is an extensive list of publications in which this method has been applied, mainly for early-type galaxies (see e.g. the compilation provided in Trager et al. 1998).

Predictions for the line-strength indices of the integrated light of stellar clusters and galaxies are obtained with stellar population synthesis models. These models calculate galaxy indices by adding the contributions of all possible stars, in proportions prescribed by stellar evolution models. The indices required of all such stars are obtained from observed stellar libraries, but since the spectra in these libraries were often noisy and did not contain all types of stars present in galaxies, people used the so-called fitting functions, which relate measured line-strength indices to the atmospheric parameters ($T_{\rm eff}$, $\log g$, [Fe/H]) of library stars. The most widely used fitting functions are those computed on the basis of the Lick/IDS stellar library (Burstein et al. 1984; Gorgas et al. 1993; Worthey et al. 1994). There are, however, alternative fitting functions in the optical range (e.g. Buzzoni 1995; Gorgas et al. 1999; Schiavon 2007; Tantalo, Chiosi & Piovan 2007) and in other spectral ranges (e.g. Cenarro et al. 2002; Mármol-Queraltó et al. 2008).

The most important parameters that can be obtained using stellar population synthesis are age (as a proxy for the star formation history) and metallicity (the average metal content). There are several methods for performing stellar population analysis based on these indices. By far the most popular method is to build key diagnostic model grids by plotting an age-sensitive indicator (e.g. Hβ) versus a metallicity-sensitive indicator (e.g. Mgb, $\langle$Fe$\rangle$), to estimate the age and metallicity (e.g. Trager et al. 2000; Kuntschner et al. 2006). There are other methods that, for example, employ as many Lick indices as possible and simultaneously fit them in a χ^2 sense (e.g. Vazdekis et al. 1997; Proctor, Forbes & Beasley 2004). An alternative method is the use of principal component analysis (e.g. Covino, Galletti & Pasinetti 1995; Wild et al. 2009).

In the last decade, the appearance of a generation of stellar population models that predict full spectral energy distributions (SEDs) at moderately high spectral resolution has provided new means for improving the stellar population analysis (e.g. Vazdekis 1999, hereafter V99; Bruzual & Charlot 2003; Le Borgne et al. 2004). These models employ newly developed extensive empirical stellar spectral libraries with flux-calibrated spectral response and good atmospheric parameter coverage. Among the most popular stellar libraries are those of Jones (1999), CaT (Cenarro et al. 2001a), ELODIE (Prugniel & Soubiran 2001), STELIB (Le Borgne et al. 2003), INDO-US (Valdes et al. 2004) and Medium resolution INT Library of Empirical Spectra (MILES; Sánchez-Blázquez et al. 2006a, hereafter SB06a). Models that employ such libraries are those of, e.g., V99, Vazdekis et al. (2003, hereafter V03), Bruzual & Charlot (2003) and Le Borgne et al. (2004). Alternatively, theoretical stellar libraries at high spectral resolutions have also been developed for this purpose (e.g. Murphy & Meiksin 2004; Zwitter, Castelli & Munari 2004; Coelho et al. 2005; Munari et al. 2005; Rodríguez-Merino et al. 2005; Martins & Coelho 2007). Some examples of models that use such libraries are Schiavon, Barbuy & Bruzual (2000), González-Delgado et al. (2005) and Coelho et al. (2007).

There are important limitations inherent to the method that prevent us from easily disentangling relevant stellar population parameters. The most important one is the well-known age/metallicity degeneracy, which affects not only colours but also absorption-line-strength indices (e.g. Worthey 1994). This degeneracy is partly due to the isochrones and partly due to the fact that line-strength indices change with both age and metallicity. The effects of this degeneracy are stronger when low-resolution indices are used, as the metallicity lines appear blended. Alternative indices that were thought to work at higher spectral resolutions, such as those of Rose (1985, 1994), have been proposed to alleviate the problem.

New indices with greater abilities to lift the age/metallicity degeneracy have been proposed with the aid of the new full-SED models (e.g. Vazdekis & Arimoto 1999; Bruzual & Charlot 2003; Cervantes & Vazdekis 2009). These models allow us to analyse the whole information contained in the observed spectrum at once. In fact, there is a growing body of full spectrum fitting algorithms that are being developed for constraining and recovering in part the star formation history (e.g. Panter, Heavens & Jimenez 2003; Cid Fernandes et al. 2005; Ocvirk et al. 2006a,b; Koleva et al. 2008). Furthermore the use of these single-metallicity stellar population (SSP) SEDs, which have sufficiently high spectral resolution, has been shown to significantly improve the analysis of galaxy kinematics both in the optical (e.g. Sarzi et al. 2006) and in the near-IR (e.g. Falcón-Barroso et al. 2003), for both absorption and emission lines.

Here we present single-age, SSP SEDs based on the empirical stellar spectral library MILES that we presented in SB06a and Cenarro et al. (2007, hereafter C07a). These models represent an extension of the V99 SEDs to the full optical spectral range. These MILES models are meant to provide better predictions in the optical range for intermediate and old stellar populations. In SB06a we provided all relevant details for MILES, which has been obtained at the 2.5 m Issac Newton Telescope (INT) at the Observatorio del Roque de Los Muchachos, La Palma. The library is composed of 985 stars covering the spectral range $\lambda\lambda$3540–7410 Å at 2.3 Å (FWHM). MILES stars were specifically selected for population synthesis modelling. In C07a, we present a homogenized compilation of the stellar parameters ($T_{\rm eff}$, $\log g$, [Fe/H]) for the stars of this library. In fact, the parameter coverage of MILES constitutes a significant improvement over previous stellar libraries and allows the models to safely extend the predictions to intermediate-aged stellar populations and to lower and higher metallicities.

The models that we present here are based on an empirical library, i.e. observed stellar spectra, and therefore the synthesized SEDs are imprinted with the chemical composition of the solar neighbourhood, which is the result of the star formation history experienced by our Galaxy. As the stellar isochrones (Girardi et al. 2000) – i.e. the other main ingredient feeding the population synthesis code

– are solar-scaled, our models are self-consistent and scaled-solar for solar metallicity. In the low metallicity regime, however, our models combine scaled-solar isochrones with stellar spectra that do not show this abundance ratio pattern (e.g. Edvardsson et al. 1993; Schiavon 2007). In the second paper of this series we will present self-consistent models, both scaled-solar and α-enhanced, for a range in metallicities. For this purpose we have used MILES, together with theoretical model atmospheres, which are coupled to the appropriate stellar isochrones.

We note, however, that the use of our (base) models, which are not truly scaled-solar for low metallicities, does not affect in a significant manner the metallicity and age estimates obtained from galaxy spectra in this metallicity regime (e.g. Michielsen et al. 2008). For the high metallicity regime, where massive galaxies reside and show enhanced [Mg/Fe] ratios, the observed line strengths for various popular indices (e.g. Mg*b*, Fe5270) are significantly different from the scaled-solar predictions. It has been shown that by changing the relative element abundances, and making them α-enhanced, both the stellar models (e.g. Salaris, Groenewegen & Weiss 2000) and the stellar atmospheres (e.g. Tripicco & Bell 1985; Korn, Maraston & Thomas 2005; Coelho et al. 2007) are affected. However it has also been shown that base models, such as the ones we are presenting here, can be used to obtain a good proxy for the [Mg/Fe] abundance ratio, if appropriate indices are employed for the analysis (e.g. Yamada et al. 2006). In fact we confirm the results of, e.g., Sánchez-Blázquez et al. (2006c), de la Rosa et al. (2007) and Michielsen et al. (2008), who obtain a linear relation between the proxy for [Mg/Fe], obtained with scaled-solar models, and the abundance ratio estimated with the aid of models that specifically take into account non-solar element mixtures (e.g. Tantalo, Chiosi & Bressan 1998; Thomas, Maraston & Bender 2003; Lee & Worthey 2005; Graves & Schiavon 2008).

In Section 2, we describe the main model ingredients, the details of the stellar spectral library MILES and the steps that have been followed for its implementation in the stellar population models. In Section 3, we present the new single-age, single-metallicity SSP SEDs and provide a quantitative analysis for assessing their quality. In Section 4, we show line-strength indices as measured on the newly synthesized SSP spectra and propose a new reference system as an alternative to the Lick/IDS system, to work with these indices. In Section 5, we provide a discussion about the colours measured on the new SSP SEDs. In Section 6, we apply these models to a set of representative stellar clusters and galaxies to illustrate the capability of the new models. In Section 7, we present a web page to facilitate the use and handling of our models. Finally, in Section 8 we provide a summary.

2 MODELS

The SSP SEDs presented here represent an extension to the full optical spectral range of the V99 models, as updated in V03. We briefly summarize here the main ingredients and the relevant aspects of this code.

2.1 Main ingredients

We use the solar-scaled theoretical isochrones of Girardi et al. (2000). A wide range of ages and metallicities are covered, including the latest stages of stellar evolution. A synthetic prescription is used to include the thermally pulsing asymptotic giant branch (AGB) regime to the point of complete envelope ejection. The isochrones are computed for six metallicities $Z = 0.0004$, 0.001, 0.004, 0.008, 0.019 and 0.03, respectively, where 0.019 represents the solar value. In addition, we include an updated version of the models published in (Girardi et al. 1996) for $Z = 0.0001$. The latter calculations are now compatible with Girardi et al. (2000). The range of initial stellar masses extends from 0.15 to 7 $M_\odot$. The input physics of these models has been updated with respect to Bertelli et al. (1994) with an improved version of the equation of state, the opacities of Alexander & Ferguson (1994) [which result in a red giant branch (RGB) that is slightly hotter than in Bertelli et al.] and a milder convective overshoot scheme. A helium fraction was adopted according to the relation: $Y \approx 0.23 + 2.25Z$. For the thermally-pulsing (TP)-AGB phase Girardi et al. (2000) adopt a simple synthetic prescription that, for example, does not take into account the third dredge-up. An improved treatment for this difficult stellar evolutionary phase has been recently included by Marigo et al. (2008). The effects of such improvements become relevant for the near-IR spectral range (see e.g. Maraston 2005; Marigo et al. 2008).

The theoretical parameters of the isochrones $T_{\rm eff}$, $\log g$, [Fe/H] are transformed to the observational plane by means of empirical relations between colours and stellar parameters (temperature, metallicity and gravity), instead of using theoretical stellar atmospheres. We mostly use the metallicity-dependent empirical relations of Alonso, Arribas & Martínez-Roger (1996, 1999; respectively, for dwarfs and giants). Each of these libraries is composed of $\sim$500 stars and the temperature scales obtained are based on the IR-flux method, i.e. only marginally dependent on model atmospheres. We use the empirical compilation of Lejeune, Cuisinier & Buser (1997, 1998) (and references therein) for the coolest dwarfs ($T_{\rm eff} \leq 4000$ K) and giants ($T_{\rm eff} \leq 3500$ K) for solar metallicity. For these low temperatures, we use a semi-empirical approach to other metallicities on the basis of these relations and the model atmospheres of Bessell et al. (1989, 1991) and the library of Fluks et al. (1994). The empirical compilation of Lejeune, Cuisinier & Buser (1997, 1998) was also used for stars with temperatures above $\sim$8000 K. We apply the metal-dependent bolometric corrections (BC) given by Alonso, Arribas & Martínez-Roger (1995, 1999; respectively, for dwarfs and giants). For the Sun, we adopt $\rm BC_\odot = -0.12$ and a bolometric magnitude of 4.70.

We have computed our predictions for several initial mass functions (IMFs): the two power-law IMFs described in Vazdekis et al. (1996) (i.e. unimodal and bimodal), which are characterized by its slope μ as a free parameter, and the multipart power-law IMFs of Kroupa (2001) (i.e. universal and revised). In our notation, the Salpeter (1955) IMF corresponds to a unimodal IMF with $\mu = 1.3$. Further details of the IMF definitions are given in appendix A of V03. We set the lower and upper mass cut-offs of the IMF to 0.1 and 100 $M_\odot$, respectively.

2.2 MILES stellar library

To compute the SSP SEDs in the full optical spectral range we use the MILES library, whose main characteristics are given in SB06a. The stars of the library were selected to optimize the stellar parameter coverage required for population synthesis modelling. This is, in fact, one of the major advantages of this library. Another important feature of the library is that the stellar spectra were carefully flux-calibrated. To reach this goal, all the stars were observed through a wide (6 arcsec) slit to avoid selective flux losses due to the differential refraction effect, in addition to the higher resolution set-ups used to achieve the blue and red parts of the stellar spectra. Telluric absorptions that were present in the redder part of the spectra were

properly removed. We refer to SB06a for the technical details on how these aspects were tackled.

To prepare this library for its implementation in the models, we identified those stars whose spectra might not be properly representative of a given set of atmospheric parameters. We used the SIMBAD data base for identifying the spectroscopic binaries in the MILES sample. A number of these stars were removed from the original sample as they were found to be non-essential since MILES contains sufficient stars with similar atmospheric parameters. We also checked for those stars with a high signal of variability ($\Delta V > 0.10$ mag), according to the Combined General Catalogue of Variable Stars of Kholopov et al. (1998) (the electronically readable version provided at CDS). Some stars with signs of variability were removed, when no such high variability was expected according to their spectral types and atmospheric parameters and, at the same time, we were able to identify alternative stars in the library with similar parameters and no such sign of variability. Various stars were discarded because emission lines were detected in their spectra. For various technical reasons, we also discarded from the original MILES list an additional number of stars: those with a very low signal-to-noise ratio (S/N) in the blue part of the spectrum or for which the atmospheric parameters were lacking or had problems in the continuum.

Each stellar spectrum of this selected subsample of stars was compared to a synthetic spectrum of similar atmospheric parameters computed with the algorithm described in V03 (Appendix B) (see also Section 2.3) employing the MILES stellar library. To perform this test, we first excluded from the list the target star for which we wished to synthesize a similar spectrum. We then compared the synthesized stellar spectrum with the observed one. This comparison was found to be very useful for identifying stellar spectra with possible problems and, eventually, discard them. In case of doubt, particularly for those regions of parameter space with poorer coverage, we compared the observed spectrum of our star with the spectra of those stars, with the closest atmospheric parameters, which were selected by the algorithm to synthesize our target star. As an example of this method, Fig. 1 shows the results for stars of varying temperatures, gravity and metallicities.

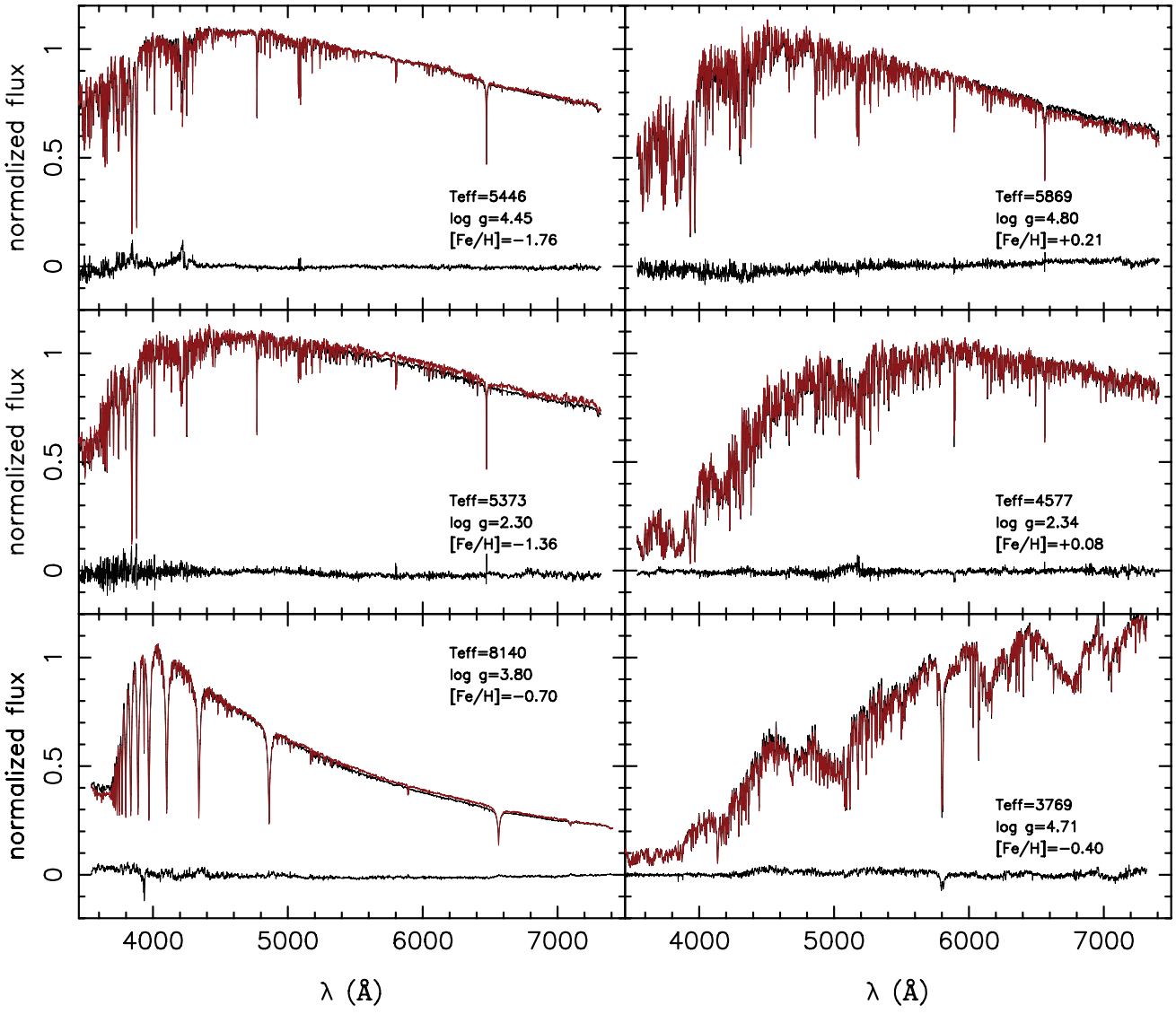

Figure 1. MILES stars for various representative spectral types are plotted in the different panels in black. In each panel, we overplot the spectrum corresponding to a star with identical atmospheric parameters that we have computed on the basis of the MILES data base (except for the star itself) following the algorithm described in Section 2.3. The residuals are given in the bottom of each panel. (see the text for details).

According to these careful inspections and tests, we marked 135 stars of the MILES data base. While 60 of these stars were removed from the original sample, we kept 75 stars, which were found to be useful for improving the coverage of certain regions of parameter space. For the latter, however, we decreased the weight with which they contribute when we synthesize a stellar spectrum for a given set of atmospheric parameters. In practice this is performed by artificially decreasing their S/N, according to the prescription adopted in Section 2.3. For the interested reader, we provide explanatory notes for these stars in an updated table of the MILES sample that can be found in http://miles.iac.es.

2.2.1 *Stellar atmospheric parameter coverage*

Fig. 2 shows the parameter coverage of the selected subsample of MILES stars for dwarfs and giants (separated at $\log g = 3.0$) compared with the original MILES sample. The 75 stars with decreased weights are also indicated. The parameters of MILES plotted here are the result of an extensive compilation from the literature, homogenized by taking as a reference the stars in common with Soubiran, Katz & Cayrel (1998), which have very well-determined atmospheric parameters. We refer the reader to C07a for an extensive description of the method and the adopted parameters. For comparison, we show the parameter coverage of some popular stellar libraries (STELIB: Le Borgne et al. 2003; Lick/IDS: Gorgas et al. 1993; Worthey et al. 1994; INDO-US: Valdes et al. 2004; and ELODIE 3.1: Prugniel et al. 2007). For ELODIE 3.1, we use the parameters determined with the TGMET software (see Prugniel & Soubiran 2004 for details) to maximize the number of plotted stars. We adopt the mean value for those stars with repeated observations.

Fig. 2 shows that, at solar metallicity, all types of stars are well represented in all libraries. At lower metallicities, however, MILES shows much better coverage of the parameter space for both dwarfs and giants than other libraries. Particularly relevant is the presence of dwarfs with temperatures above $T_{\rm eff} > 6000$ K and metallicities $[{\rm M/H}] < -0.5$. With these stars, we are in a position to overcome a major limitation of current population synthesis models based on empirical stellar libraries providing us with predictions for metal-poor stellar populations in the age range of 0.1–5 Gyr. Furthermore, there are sufficient stars to compute models for metallicities as low

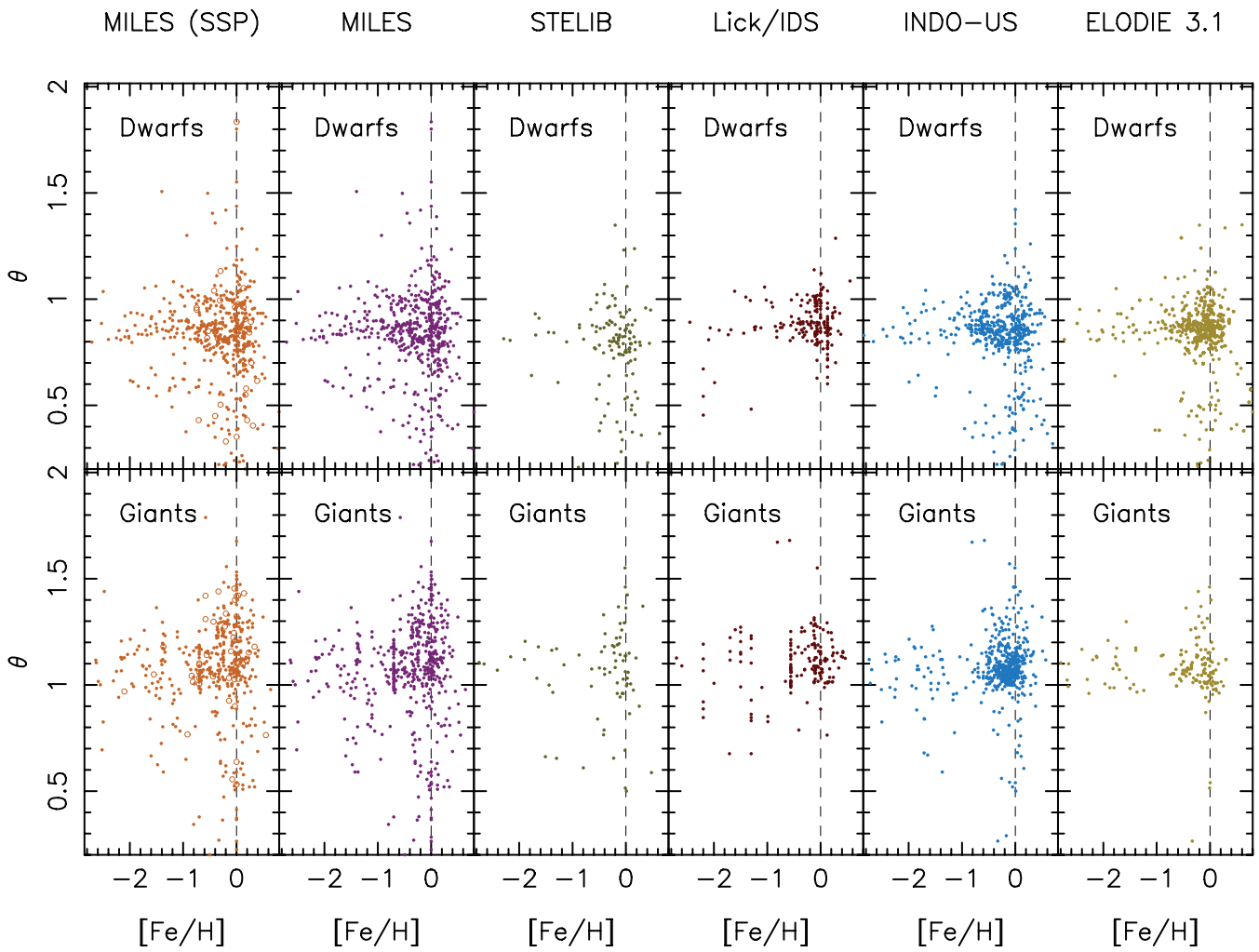

Figure 2. The fundamental parameter coverage of the subsample of selected MILES stars is shown in the left-hand panels for dwarfs (top) and giants (bottom). Stars with decreased weights are plotted with open circles. The parameters of the original MILES sample are plotted in the second column of the panels. We show, for comparison, the parameter coverage of various popular stellar libraries (STELIB, Lick, INDO-US and ELODIE). For reference, we indicate in each panel the solar metallicity (thin dashed vertical line).

as [M/H] = −2.3, particularly for very old stellar populations where the temperature of the turnoff is lower.

Another advantage with respect to the other libraries is the coverage of metal-rich dwarf and giant stars that allow us to safely compute SSP SEDs for [M/H] = +0.2. Also for even higher metallicities MILES shows good stellar parameter coverage and therefore it is possible to compute SEDs for [M/H] $\sim$ +0.4. These predictions will be presented – and we will make them available in our website – in a future paper, where we feed the models with the Teramo isochrones (Pietrinferni et al. 2004), which reach these high metallicity values.

These super-solar metallicity predictions are particularly relevant for studying massive galaxies and it is for the first time that they can be safely computed, without extrapolating the behaviour of the spectral characteristics of the stars at higher metallicities as is done, e.g., in models based on the Lick/IDS empirical fitting functions (e.g. Worthey 1994; Thomas et al. 2003). Finally, it is worth noting that these new model predictions also extend the range of SSP metallicities and ages of our previous model SEDs based on the Jones (1999) (V99) and Cenarro et al. (2001a) (V03) stellar libraries. A quantitative analysis of the quality of the models based on the atmospheric parameter coverage of the employed libraries is provided in Section 3.2.

2.3 SSP spectral synthesis

We use the method described in V99 and V03 for computing the SSP SEDs on the basis of the selected subsample of MILES stars. In short, we integrate the spectra of the stars along the isochrone taking into account their number per mass bin according to the adopted IMF. For this purpose, each requested stellar spectrum is normalized to the corresponding flux in the V band, following the prescriptions adopted in our code, which are based on the photometric libraries described in Section 2.1. We refer the interested reader to the papers previously mentioned for a full description of the method.

The SSP SED, $S_\lambda(t, [\mathrm{M/H}])$, is calculated as follows:

$$S_\lambda(t, [\mathrm{M/H}]) = \int_{m_\mathrm{l}}^{m_\mathrm{t}} S_\lambda(m, t, [\mathrm{M/H}]) N(m, t) \times F_V(m, t, [\mathrm{M/H}]) \mathrm{d}m, \quad (1)$$

where $S_\lambda(m, t, [\mathrm{M/H}])$ is the empirical spectrum, normalized in the V band, corresponding to a star of mass m and metallicity [M/H], which is alive at the age assumed for the stellar population t. $N(m, t)$ is the number of this type of star, which depends on the adopted IMF. m_l and m_t are the stars with the smallest and largest stellar masses, respectively, which are alive in the SSP. The upper mass limit depends on the age of the stellar population. Finally, $F_V(m, t, [\mathrm{M/H}])$ is its flux in the V band, which comes from transforming the theoretical parameters of the isochrones. It is worth noting that the latter is performed on the basis of empirical photometric stellar libraries, as described in Section 2.1, rather than relying on theoretical stellar atmospheres, as is usually done in other stellar population synthesis codes. This avoids errors coming from theoretical uncertainties such as the incorrect treatment of convection, turbulence, non-local thermodynamic equilibrium effects, incorrect or incomplete line list, etc. (see Worthey & Lee 2006).

We obtain the spectrum for each requested star with a given atmospheric parameter interpolating the spectra of adjacent stars using the algorithm described in V03. The code identifies the MILES stars whose parameters are enclosed within a given box around the point in parameter space (θ_0, $\log g_0$, $[\mathrm{M/H}]_0$). When needed, the box is enlarged in the appropriate directions until suitable stars are found (e.g. less and more metal-rich). This is done by dividing the original box into eight cubes, all with one corner at that point. This reduces the errors in the case of gaps and asymmetries in the distribution of stars around the point. The larger the density of stars around the requested point, the smaller the box is. The sizes of the smallest boxes are determined by the typical uncertainties in the determination of the parameters (Cenarro et al. 2001b). In each of the boxes, the stars are combined taking into account their parameters and the S/N of their spectra. Finally, the combined spectra in the different boxes are used to obtain a spectrum with the required atmospheric parameters by weighting the appropriate quantity. For a full description of the algorithm, we refer the reader to V03 (Appendix B).

It is worth noting that, within this scheme, a stellar spectrum is computed according to the requested atmospheric parameters, irrespective of the evolutionary stage. We are aware that this approach is not fully appropriate for the TP-AGB phase, where O-rich stars, C-rich stars and stars in the superwind phase are present. In fact, in Mármol-Queraltó et al. (2008) we have found non-negligible differences in the CO bandhead at 2.3 μm between 19 AGB stars, all from the MILES library, and RGB stars of similar parameters. This, in principle, could introduce an error in our predictions as very few C-rich, O-rich or superwind phase TP-AGB stars can be found in MILES. However, the contribution of such stars to the total flux budget in the V band is just a few per cent, mainly for stellar populations of intermediate ages (0.1–1.5 Gyr; see e.g. Bruzual 2007).

2.3.1 Effects of systematic variations in the adopted stellar parameters

Percival & Salaris (2009) have recently shown that systematic uncertainties associated with the three fundamental stellar atmospheric parameters might have a non-negligible impact on the resulting SSP line-strength indices. The interested reader is referred to that paper for details and for a suite of tests showing the effects of varying these parameters.

In particular, a relatively small offset in the effective temperature of 50–100 K, which is of the order of the systematic errors in the conversion from temperature to colours used here (Alonso et al. 1996), may change the age of a 14 Gyr stellar population by 2–3 Gyr and alleviate the so-called zero-point problem for which the ages of the globular clusters (GCs) are older than the most recent estimations of the age of the Universe. Furthermore, they show that, in many cases, there is a mismatch in scales between the underlying models (the isochrones) and the adopted stellar library in the stellar population models. We already showed in C07a that the Alonso et al. (1996, 1999) photometric library did not show any offset with the MILES atmospheric parameters. Therefore, there is no mismatch in scales between the models and the stellar library in the models presented here.

However, inspired by this work we decided to compare our stellar parameters with those from several recently published works (e.g. Ramírez & Meléndez 2005; Casagrande et al. 2006; González-Hernández & Bonifacio 2009), to see if our parameters should be corrected. We show here, for illustrative purposes, the comparison of our parameters with those using the new temperature scale of González-Hernández & Bonifacio (2009), whom derived Teff using the IR flux method (Blackwell et al. 1990), as it is the work with a larger number of stars in common with MILES (215) and because it is the one showing larger differences.

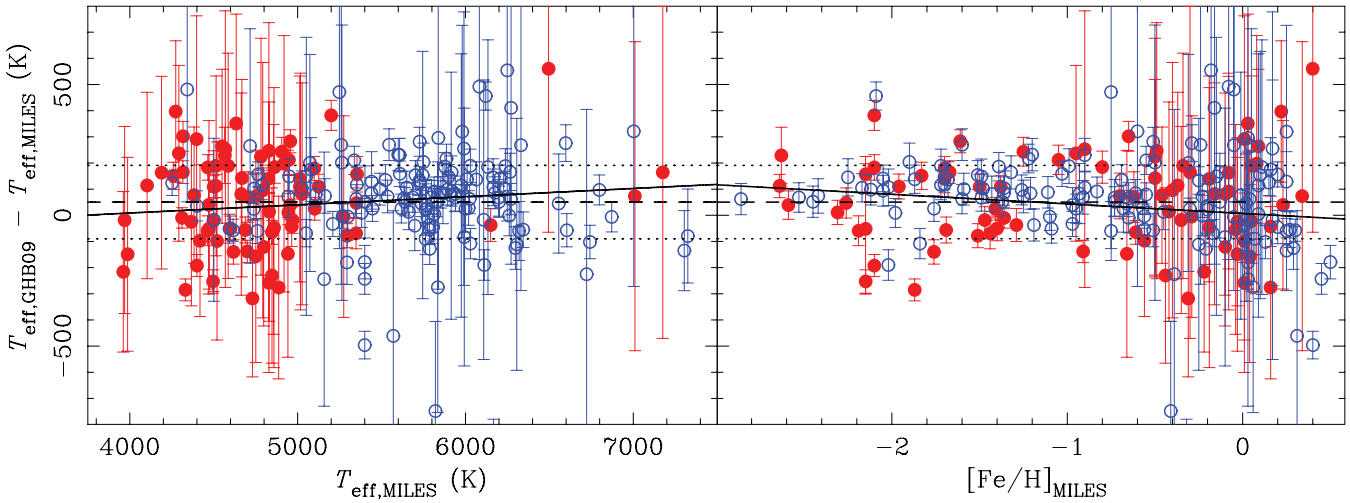

Figure 3. Comparison of MILES temperatures with those of González-Hernández & Bonifacio (2009) as a function of temperature (left-hand panel) and metallicity (right-hand panel). Giants are represented by red solid circles (81 stars) whereas dwarfs are represented by open blue circles (134 stars). The error weighted linear fit to all the stars is plotted in the two panels with a solid line. The dashed line in each panel shows the mean error weighted offset obtained from all the stars $\Delta T_{\rm eff} = 51(\pm 10)$ K, whereas the dotted lines represent the standard deviation (140 K) from this offset.

In Fig. 3, we plot the difference in temperature for the dwarf and giant stars in common between González-Hernández & Bonifacio (2009) and MILES as a function of temperature and metallicity. We performed linear fits weighted with the errors obtaining the following relations:

$$\Delta T_{\rm eff} = -116(\pm 80) + 0.0312(\pm 0.0148) T_{\rm eff\,MILES} \quad (2)$$

and metallicity

$$\Delta T_{\rm eff} = 7(\pm 17) - 36.56(\pm 11.79)[{\rm Fe/H}] \quad (3)$$

obtaining an rms of 138 K in the two cases. The mean temperature offsets of 59 and 54 K are for dwarfs and giants, respectively. This is in good agreement with the offsets obtained by González-Hernández & Bonifacio (2009) when comparing their temperature scale with that of Alonso et al. (1996, 1999). Finally, we did not find any significant offset in metallicity or gravity among these samples.

We computed an alternative SSP model SED library by transforming the MILES temperatures to match this scale. These models can be used to better assess the uncertainties involved in the method. We comment on these models in Sections 5 and 6.1.1. However, we do not find any strong reason for adopting the González-Hernández & Bonifacio (2009) model since its accuracy at high metallicities is worse than in the Alonso et al. (1996, 1999) model [the temperature scale of González-Hernández & Bonifacio (2009) has been optimized for low metallicities while the errors in the temperature determination for metal-rich giant stars are very large]. Furthermore, as we have already mentioned above, the temperature scales of the isochrones and stellar libraries in our models do not show any offset.

3 MILES SSP SEDS

Table 1 summarizes the spectral properties of the newly synthesized SSP SEDs. The nominal resolution of the models is FWHM = 2.3 Å, which is almost constant along the spectral range. For applications requiring to know the resolution with much greater accuracy, we refer the reader to fig. 4 of SB06a. This resolution is poorer than that of the models we presented in V99 (FWHM = 1.8 Å), but this is compensated by the large spectral range λλ3540.5–7409.6 Å, with

Table 1. Spectral properties and parameter coverage of the synthesized MILES SSP SEDs.

Spectral properties	
Spectral range	λλ3540.5–7409.6 Å
Spectral resolution	FWHM = 2.3 Å, σ = 54 km s^{-1}
Linear dispersion	0.9 Å pixel^{-1} (51.5 km s^{-1})
Continuum shape	Flux-scaled
Telluric absorption residuals	Fully cleaned
Units	F_λ/L$_\odot$ Å^{-1} M$_\odot^{-1}$, L$_\odot$ = 3.826 × 10^{33} erg s^{-1}
SSPs parameter coverage	
IMF type	Unimodal, bimodal, Kroupa universal, Kroupa revised
IMF slope (for unimodal and bimodal)	0.3–3.3
Stellar mass range	0.1–100 M$_\odot$
Metallicity	−2.32, −1.71, −1.31, −0.71, −0.41, 0.0, +0.22
Age ([M/H] = −2.32)	10.0 < t < 18 Gyr (only for IMF slopes ≤ 1.8)
Age ([M/H] = −1.71)	0.07 < t < 18 Gyr
Age (−1.31 ≤ [M/H] ≤ +0.22)	0.06 < t < 18 Gyr

flux-calibrated response and no telluric residuals. For computing the SEDs, we have adopted a total initial mass of $1\,M_{\odot}$. Table 1 also summarizes the SSP parameters for which our predictions can be safely used. We discuss this issue in Section 3.2.

3.1 Behaviour of the SSP SEDs

In Fig. 4, we show the new spectral library of SSP models for different ages and metallicities. All the spectra are plotted at the nominal resolution of the models (FWHM = 2.3 Å). The SSP age sequence shows a weaker 4000 Å break and stronger Balmer line strengths as the age decreases. The largest Balmer line strengths, however, are reached for ages of ∼0.4 Gyr. On the other hand, the metallic absorption lines become more prominent with an increasing age. It can be seen that the continuum of the models with larger ages is heavily lowered by the strengthening of the metallic features (line blanketing). This is the reason why the Lick/IDS indices were defined using pseudo-continua instead of real continua (Worthey et al. 1994). In the SSP SED metallicity sequence, it can be seen that Balmer line strengths decrease and metallicity-sensitive features get stronger for increasing metallicity. These two SSP SED sequences clearly illustrate the effects of the age/metallicity degeneracy.

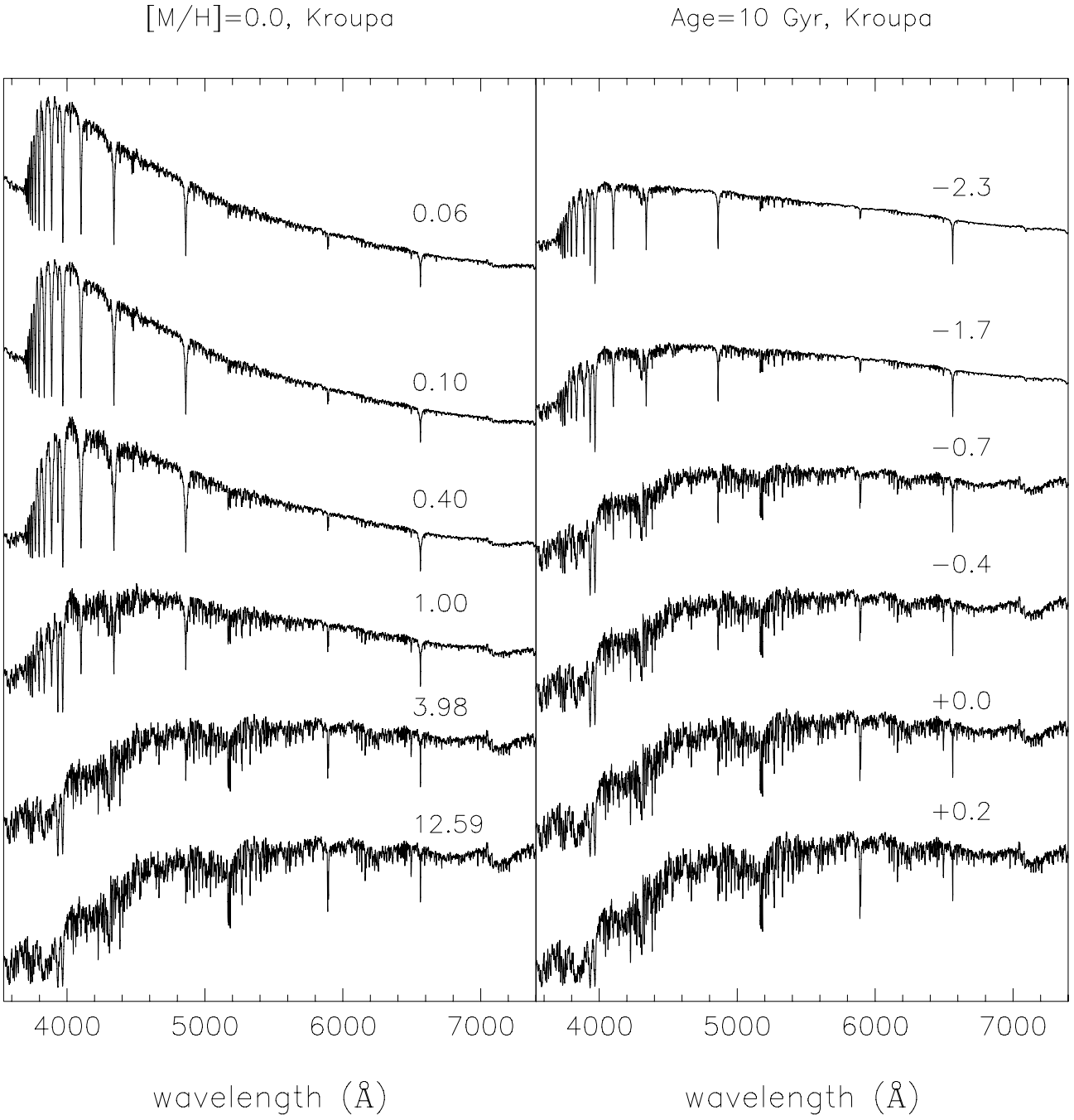

Figure 4. Left-hand panel: solar metallicity SSP spectra of different ages (in Gyr), increasing from top to bottom. Right-hand panel: SSP spectra of 10 Gyr and different metallicities, increasing from top to bottom. All the SSP spectra are plotted at the nominal resolution of the models (i.e. FWHM = 2.3 Å). All these models are computed adopting a Kroupa universal IMF. For clarity, the SSP spectra have been shifted by arbitrary amounts.

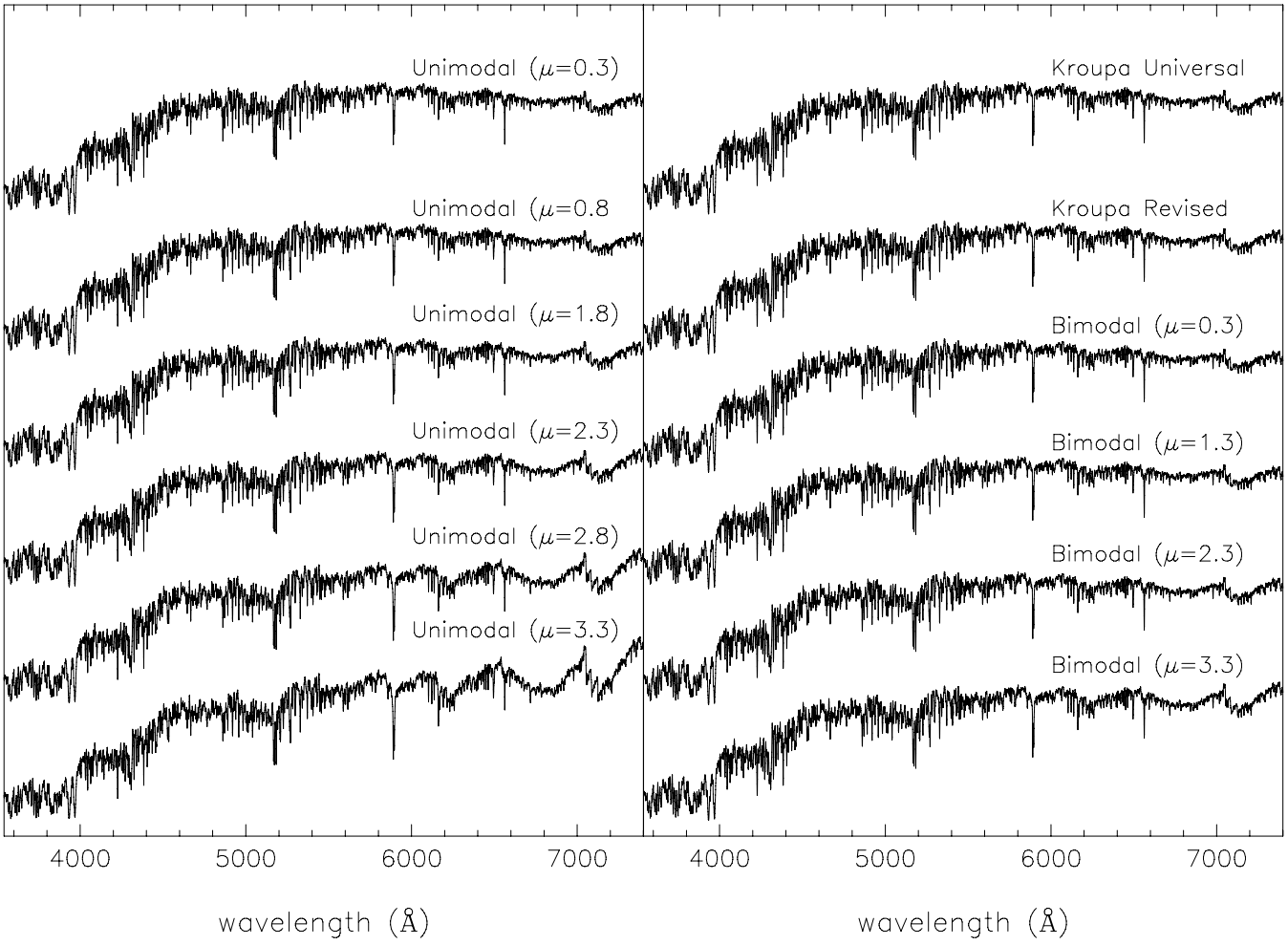

Figure 5. Left-hand panel: solar metallicity SSP spectra of 10 Gyr, computed using a unimodal IMF of an increasing slope from top to bottom. The Salpeter case, i.e. $\mu = 1.3$, has been plotted in the right-hand panel of Fig. 4. The SSP spectra are plotted at the nominal resolution of the models (i.e. FWHM = 2.3 Å). Right-hand panel: solar metallicity SSP spectra of 10 Gyr for different IMF shapes. From top to bottom: Kroupa universal, Kroupa revised and bimodal with increasing slopes, as indicated in the panel. All the spectra have been shifted by arbitrary amounts for clarity.

In Fig. 5, we illustrate the effects of varying the IMF slope (μ) and the IMF shape. The left-hand panel shows a sequence of SSP spectra of solar metallicity and 10 Gyr, where the slope is varied for the unimodal IMF. For old stellar populations, this IMF type shows the largest variations as the fraction of low-mass stars vary dramatically when varying the IMF slope. We see that the reddest part of the spectrum shows the highest sensitivity to this parameter. These variations do no evolve linearly as a function of μ. In fact, the SSP SEDs corresponding to the flatter IMFs look rather similar. On the other hand, the effects caused by varying μ quickly become stronger for the steepest IMFs, notably redwards of ∼5500 Å, including the Na line at ∼5800 Å and the TiO molecular band around ∼6200 and ∼6800 Å. The right-hand panel shows that the effects of varying the IMF slope are much less significant for the bimodal IMF. This is because for this IMF type, the contribution from stars with masses lower than $0.6\,\mathrm{M}_{\odot}$ is decreased. Since this IMF more closely resembles the Kroupa IMFs, it is probably more realistic. Finally, we note that the SSP SEDs for the two Kroupa (2001) IMFs and the bimodal IMF with slope 1.3 (as well as the Salpeter IMF) do not show significant differences.

3.2 Reliability of the SSP SEDs

In this section, we try to provide some quantitative way of estimating the reliability and the quality of the synthesized SSP SEDs and to estimate the size of the errors due to incomplete coverage of the stellar parameter space of the input library. We perform this evaluation as a function of the SSP age, metallicity and IMF. To do this, we have taken advantage of our algorithm for synthesizing a representative stellar spectrum for a given set of atmospheric parameters (see Section 2.3) to compute for each SSP a parameter, Q, as follows:

$$Q = \frac{\sum_{i=1}^{n_{m_t}} \left[\frac{x_s \sum_{j=1}^{8} N_i^j}{\sum_{j=1}^{8} \sqrt{\left(\frac{\phi_{\theta_i}^{\ j}}{\sigma_{\theta_m}}\right)^2 + \left(\frac{\phi_{\log g_i}^{\ j}}{\sigma_{\log g_m}}\right)^2 + \left(\frac{\phi_{[M/H]_i}^{\ j}}{\sigma_{[M/H]_m}}\right)^2}} \right] N_i F_{Vi}}{\sum_{i=1}^{n_{m_t}} N_i F_{Vi}}. \quad (4)$$

We integrate the term enclosed within the square brackets along the isochrone, from the smallest stellar mass, m_l, to the most massive star, m_t, which is alive at the age of the stellar population t, weighted by the flux in the V band, F_{Vi}, and the number of stars,

N_i, according to the adopted IMF. N_i^j is the number of stars that have been found within cube j in parameter space (where $j = 1, \ldots, 8$; see Section 2.3). For a star with given θ, $\log g$ and [M/H], the size of these cubes is given by $\phi_{\theta_i}^j$, $\phi_{\log g_i}^j$ and $\phi_{[\mathrm{M/H}]_i}^j . \sigma_{\theta_\mathrm{m}}$, $\sigma_{\log g_\mathrm{m}}$ and $\sigma_{[\mathrm{M/H}]_\mathrm{m}}$ are the minimum uncertainties in the determination of θ, $\log g$ and [M/H], respectively. Following V03, we adopt $\sigma_{\theta\,\mathrm{m}} = 0.009$, $\sigma_{\log g\,\mathrm{m}} = 0.18$ and $\sigma_{[\mathrm{M/H}]\mathrm{m}} = 0.09$. The size of the smallest cube is obtained by multiplying the minimum uncertainty by the factor x_s. Therefore, according to the square-bracketed term, for each star along the isochrone, the larger the total number of stars found in these eight cubes and the smaller the total volume, the higher the quality of the synthesized stellar spectrum.

We also compute, for each SSP, the minimum acceptable value for this parameter, Q_m. Our algorithm ensures that at least we find stars in three (out of eight) cubes to synthesize a stellar spectrum (see appendix B of V03 for details). Furthermore, the maximum enlargement that is allowed for each cube is assumed to be one-tenth of the total range covered by the stellar parameters in our library. Therefore, the sizes for the largest cubes are $\sigma_{\theta M} = 0.17$, $\sigma_{\log gM} = 0.51$ and $\sigma_{[\mathrm{M/H}]M} = 0.41$. Note that for σ_θ we also assume the condition that $60 \leq T_\mathrm{eff} \leq 3350\,\mathrm{K}$, which corresponds to the adopted σ_θ limiting values when transforming to the T_eff scale. Therefore, to compute Q_m we will assume for each stellar spectrum along the isochrone the following three conditions that must be satisfied: (i) we find stars in three cubes, (ii) there is a single star for each of these three cubes, which implies that $N_m = \sum_{j=1}^{8} N_i^j = 3$, and (iii) it is necessary to open the size of these cubes, generically, $f_p \times \sigma_{pM}$, where $f_p = 0.34$, i.e. the star is found to be located within $1\,\sigma$ of σ_{pM}, considering the two directions at either side of the requested parametric point. By substituting these values in equation (4), we obtain

$$Q_m = \frac{\frac{N_m}{8 f_p} \sum_{i=1}^{n_{m_\mathrm{t}}} \frac{N_i F_{V\,i}}{\sqrt{\left(\frac{\sigma_{\theta\,M}}{\sigma_{\theta_\mathrm{m}}}\right)^2 + \left(\frac{\sigma_{\log g\,M}}{\sigma_{\log g_\mathrm{m}}}\right)^2 + \left(\frac{\sigma_{[\mathrm{M/H}]\,M}}{\sigma_{[\mathrm{M/H}]\mathrm{m}}}\right)^2}}}{\sum_{i=1}^{n_{m_\mathrm{t}}} N_i F_{V\,i}}. \quad (5)$$

Then a quality measure of the SSP SED, due to the atmospheric parameter coverage of the stellar library feeding the models, is given by the normalized parameter

$$Q_n = \frac{Q}{Q_m}. \quad (6)$$

Although the absolute value of Q_n depends on the assumptions adopted for computing Q_m, the Q_n parameter allows us to compare the quality of a given SSP SED compared to the SEDs computed for other SSP parameters. In addition, Q_n allows us to compare the quality of SSP SEDs synthesized on the basis of different stellar spectral libraries, given the fact that the stellar spectra of these libraries are of sufficiently high quality. Furthermore, these prescriptions are the same that we use for computing a stellar spectrum of given atmospheric parameters, which have been extensively tested in V03.

Fig. 6 shows the value of Q_n as a function of the SSP age (in Gyr) for different metallicities (different line types) and adopting a unimodal IMF, with its slope increasing from the left-hand to the right-hand panel. SSP SEDs with Q_n values above 1 can be considered to be of sufficient quality, and therefore they can be safely used. The panels show that, as expected, higher quality is achieved for solar metallicity. For the Salpeter IMF, i.e. the second

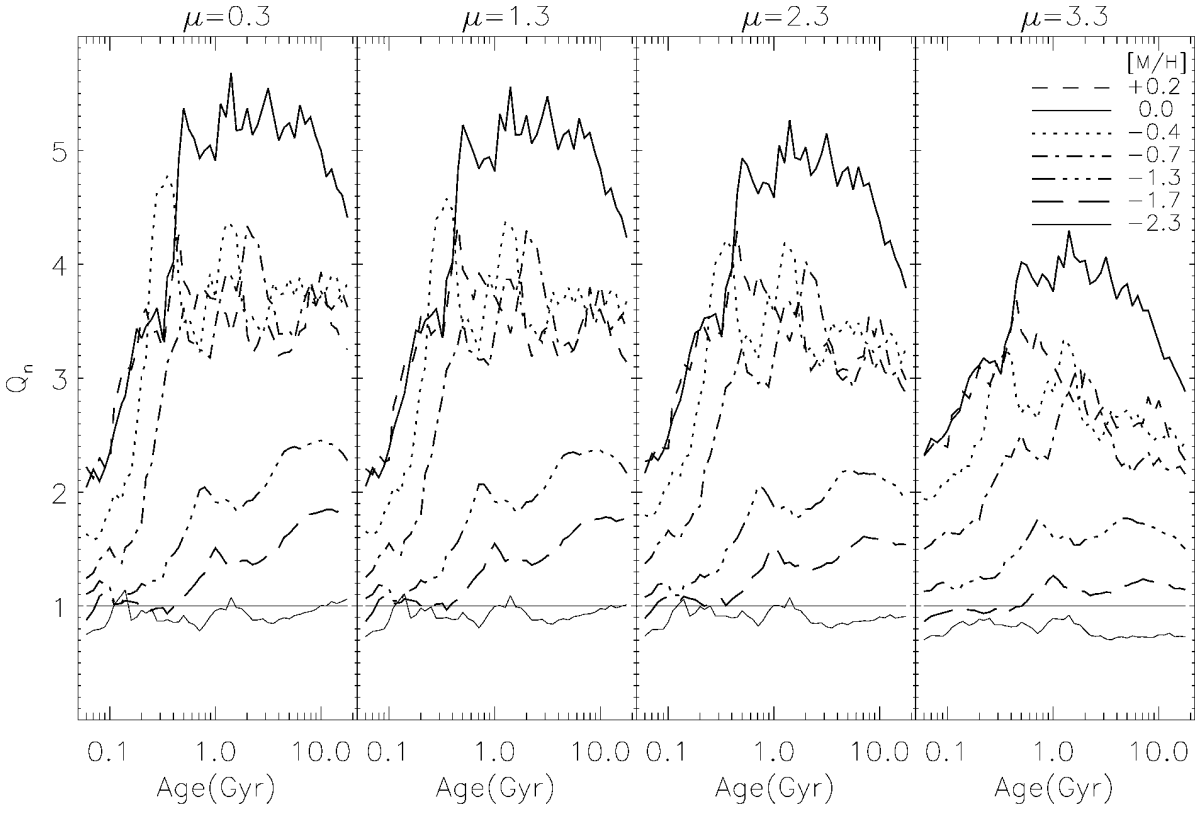

Figure 6. The quality parameter, Q_n, as a function of the SSP age (in Gyr) for different metallicities, indicated by the line types as quoted in the panels. For computing the SEDs, we use a unimodal IMF with the slope indicated on the top of each panel. SSPs with Q_n values larger than 1 can be safely used (see the text for details).

panel, Q_n reaches a value of ∼5 for stellar populations in the range of 1–10 Gyr. Outside this age range, the quality starts to decrease as low-mass and hotter MS stars are less numerous in the MILES data base.

A similar behaviour is found in Fig. 6 for the SSPs of metallicities [M/H] = +0.22, −0.41 and −0.71, all with Q_n values in the range of 3–4. Despite the fact that for all these metallicities the value of Q_n sharply decreases towards younger stellar populations, the computed SSP SEDs can be considered safe. For lower metallicities we obtain significantly lower Q_n values, which gradually decrease towards younger ages. For old stellar populations, we obtain Q_n values around 2 and around 1.5 for [M/H] = −1.31 and [M/H] = −1.71, respectively. Interestingly, according to our quantitative analysis, the SSP SEDs synthesized for [M/H] = −2.32 and ages above 10 Gyr are barely acceptable for IMFs with slopes $\mu = 0.3$ and $\mu = 1.3$. These SEDs are particularly useful for GC studies. Note the sharp increase in Q_n observed for ages around 1 Gyr. This should be mostly attributed to the fact that for stars of temperatures larger than 9000 K, we do not take into account the metallicity of the available stars for computing a stellar spectrum of given atmospheric parameters (see V03 for details). Therefore, the quality of the SEDs synthesized for the younger stellar populations is lower than that stated by Q_n.

Fig. 6 also shows that Q_n decreases slightly with an increasing IMF slope. In fact, the largest values are obtained for the flatter IMF ($\mu = 0.3$), as a result of the smaller contribution of low-mass stars, which are less abundant in MILES. This explains why Q_n drops significantly for the steepest IMF. It is worth noting that the SSP SEDs that are synthesized for the lowest metallicity cannot be considered safe for IMFs steeper than Salpeter.

For comparison we show in Fig. 7 the Q_n values obtained for two of the most popular libraries that are used in stellar population synthesis, i.e. Lick and STELIB. The first library is mainly used to predict Lick/IDS line indices via the empirical fitting functions of Worthey et al. (1994) (e.g. Worthey 1994; Vazdekis et al. 1996; Thomas et al. 2003). STELIB is the library feeding the models of Bruzual & Charlot (2003). For this purpose, we used MILES to assemble a stellar spectral library resembling Lick and another one resembling STELIB. For each of these libraries, we selected the MILES spectra for the stars in common with MILES with listed stellar parameters (i.e. 213 for Lick and 117 for STELIB). For the remaining stars, which are not available in MILES, we synthesized their spectra with our interpolating algorithm of Section 2.3, using MILES.

The two panels of Fig. 7 show that the Q_n values obtained are significantly lower than the ones obtained for MILES for all metallicities and ages. The left-hand panel shows that the SSP predictions based on the Lick library are not reliable for metallicities lower than ∼−1.3. The right-hand panel shows that this limit occurs at higher metallicity (∼−0.7) for any prediction based on STELIB. Overall the STELIB SSP models are of much lower quality than the predictions based on the Lick library, judging from the parameter coverage of these libraries. Note that there is a large dispersion in the Q_n values obtained for old stellar populations. This feature is less prominent in Fig. 6, due to the fact that the distribution of stellar parameters is far more homogeneous for MILES.

Table 1 summarizes the ranges in age, metallicity and IMF slopes for which our MILES SEDs can be considered safe. We do, however, strongly recommend to inspect Fig. 6 for a more accurate description of the quality of the SSP SEDs. Although not shown, we find that the Q_n values obtained for the two Kroupa IMF shapes and the bimodal IMF with slope 1.3 are virtually identical to those shown in the second panel of Fig. 6. For the bimodal IMF the Q_n values also decrease with an increasing IMF slope, but the effect is much lower than is the case for the unimodal IMF.

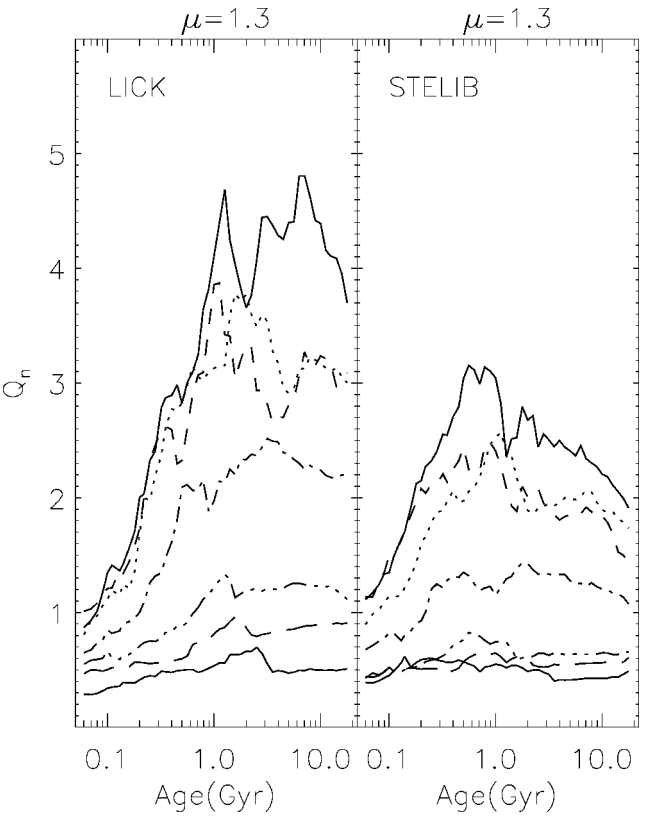

Figure 7. The same test as in Fig. 6 but for SSP SEDs computed on the basis of the atmospheric parameters corresponding to the Lick (left-hand panel) and STELIB (right-hand panel) stellar spectral libraries (see the text for details). To perform this test we selected the MILES spectra for the stars in common with MILES, whereas for the rest of the stars we synthesized their spectra with our interpolating algorithm, using the MILES spectral data base (see the text for details).

3.3 Model SED comparisons

For an extensive comparison of our newly synthesized SSP SEDs with the models of other authors, we refer the reader to the recently published paper of Koleva et al. (2008) and Cid Fernandes & González-Delgado (2010).[1] Koleva et al. compared three SSP spectral libraries: GALAXEV (Bruzual & Charlot 2003), PEGASE-HR (Le Borgne et al. 2004) and ours. Whereas the two former codes use the Padova 1994 stellar evolution models (Bertelli et al. 1994), ours employ the Padova 2000 models (Girardi et al. 2000), whose RGB is about 50–200 K hotter. Each of these codes uses different prescriptions for transforming the theoretical stellar parameters to the observational plane. The main difference is that our models mostly rely on empirical relations rather than on model atmospheres. However, the key difference between these models is the stellar libraries that they use, i.e. STELIB, ELODIE (version 3.1) and MILES for GALAXEV, PEGASE-HR and ours, respectively. Koleva et al. (2008) do this comparison by means of the full spectrum fitting approach, using two different algorithms: NBURSTS (Chilingarian et al. 2007),

[1] We provided these authors with a preliminary version of our MILES models to perform this comparison.

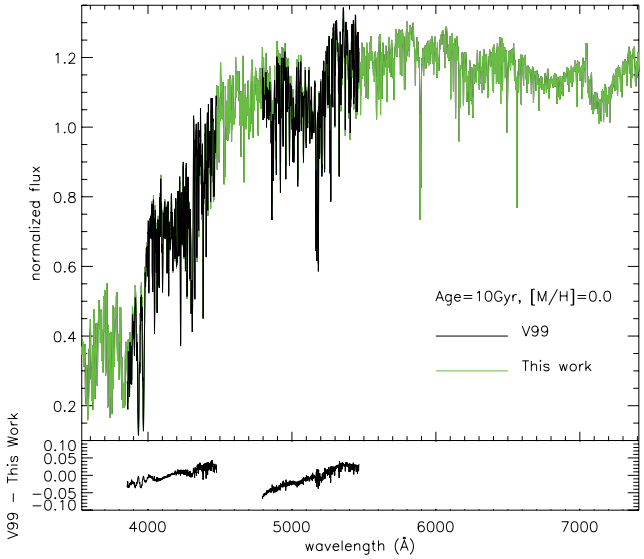

Figure 8. SSP SEDs of solar metallicity and 10 Gyr computed with the MILES (thin solid line) and Jones (1999) stellar libraries, i.e. the V99 model (thick dotted line). We adopted a unimodal IMF of slope 1.3. The V99 model, which has a higher resolution (FWHM = 1.8 Å) than MILES, was smoothed to match the resolution of the MILES model (FWHM = 2.3 Å). The residuals are plotted in the lower panel with the same scale.

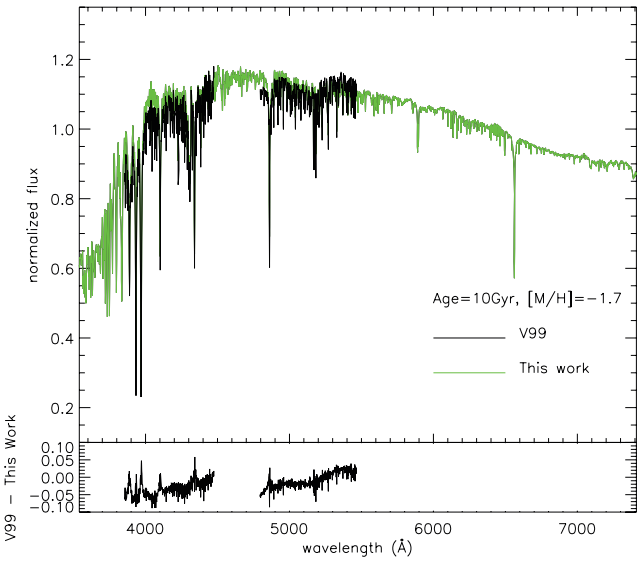

Figure 9. Similar comparison as in Fig. 8 but for metallicity [M/H] = −1.7.

which performs a parametric non-linear fit, and STECKMAP (Ocvirk et al. 2006b, a), which employs a non-parametric formalism.

Koleva et al. (2008) find that the quality of the models is very dependent on the atmospheric parameter coverage of the stellar spectral libraries. The two fitting methods show consistent results when our SEDs are compared to the PEGASE-HR SEDs, obtaining residuals of the order of 1 per cent. As expected, the largest discrepancies are found for low metallicities ([M/H] < −0.7), as shown in their fig. 2. However in our Fig. 2 we show that MILES provides significantly better coverage than ELODIE 3.1 for this low-metallicity regime for both dwarfs and giants. Furthermore, the last two panels of fig. 2 of Koleva et al. show that the discrepancy between these two model sets is larger for SSPs with ages smaller than ∼5 Gyr, which can be explained by the lack of hot metal-poor dwarfs in the ELODIE library. The fits performed by these authors reveals that the worst results are obtained when either PEGASE-HR or our models are compared with the SEDs of Bruzual & Charlot (2003). Koleva et al. conclude that this is due to the poor stellar atmospheric coverage of STELIB, particularly for the non-solar metallicity regime, as is also shown in our Fig. 2. This has been recently confirmed by Cid Fernandes & González-Delgado (2010) by comparing the model spectra to Milky Way GCs.

When comparing our MILES models with the models that we presented in V99 we show in Fig. 8 a representative SSP spectrum of solar metallicity and 10 Gyr, with the corresponding V99 model overplotted. The latter is an updated version of the original V99 models, which has been computed with the same code used to synthesize the MILES SSP SEDs. The V99 SSP spectrum, with a resolution of 1.8 Å (FWHM), was smoothed to match the resolution of the MILES model, i.e. 2.3 Å (FWHM). The residuals are plotted on a similar scale. The residuals show a systematic trend in the two narrow spectral ranges covered by the V99 models. This must be attributed to errors in the flux-calibration quality of the latter, as was reported in V99. The same pattern is seen in the residuals of Fig. 9, which shows a similar comparison at metallicity [M/H] = −1.7.

Contrary to Fig. 8, the residuals of Fig. 9 show much larger variations at shorter wavelength scales. This translates into larger index strength variations in this low metallicity regime, showing that the Jones (1999) library feeding the V99 models lacks important stars. This comparison illustrates how relevant it is to synthesize SSP SEDs with stellar libraries with good atmospheric parameter coverage, such as MILES.

4 DEFINING A NEW STANDARD SYSTEM FOR INDEX MEASUREMENTS

A major application of the SSP SEDs is to produce key line-strength indices that can be compared to the observed values. In practice, this has been the most popular approach for studying in detail the stellar content of galaxies. So far, the most widely used indices are those of the Lick/IDS system (e.g. González 1993; Vazdekis et al. 1997; Trager et al. 1998, 2000; Jørgensen 1999; Sánchez-Blázquez et al. 2003, 2006b,c,d, 2009). The standard Lick/IDS system of indices was defined on the basis of a stellar spectral library (Gorgas et al. 1993; Worthey et al. 1994), which contains about 430 stars in the spectral range λλ4000–6200 Å. The Lick/IDS system has been very popular because the stellar library contains stars with a fair range of stellar parameters and therefore is appropriate to build stellar population models. The most popular application of this library has been the use of empirical fitting functions, which relate the index strengths, measured at the Lick/IDS resolution, to the stellar atmospheric parameters. Because the value of the Lick/IDS indices depends on the broadening of the lines, authors with spectral data who wish to use the population models based on the Lick/IDS fitting functions (e.g. Worthey 1994; Vazdekis et al. 1996; Thomas et al. 2003), or compare them with previously published data, need to transform their measurements into the Lick/IDS system. As the resolution of the Lick/IDS library (FWHM ∼ 8–11 Å) is much lower than what is available with modern spectrographs, the science spectra are usually broadened to the lower Lick/IDS resolution. This is performed by convolving with a Gaussian function, whose width varies as a function of wavelength, as the resolution of the Lick/IDS system, apart from being low, also suffers from an ill-defined wavelength dependence (see Worthey & Ottaviani 1997). This effect is particularly significant for systems with small intrinsic

velocity dispersions, such as GCs and dwarf galaxies, in which part of the valuable information contained in the higher resolution galaxy spectra is lost.

After that, it is still necessary to correct the measurements for the line broadening due to the velocity dispersion of the stars in the integrated spectra of galaxies. The correction should be calculated by finding a good stellar template of the galaxy by combining an appropriate set of stellar or synthetic spectra which matches the observed spectrum. This is because this correction is highly sensitive to the strength of the index. Despite this, many studies still use a single polynomial obtained with a single star as a template, which may have very different index values than those on the observed spectra (see Kelson et al. 2006 for a discussion of the systematic effects associated with this procedure).

Due to the fact that the shape of the continuum in the Lick/IDS stars is not properly calibrated, the use of the Lick system requires a conversion of the observational data to the instrumental response curve of the Lick/IDS data set (see the analysis by Worthey & Ottaviani 1997) that will affect, predominantly, the broad indices. This is usually done by observing a number of Lick stars with the same instrumental configuration as for the science objects. Then, by comparing with the tabulated Lick index measurements, the authors find empirical correction factors for each index. This experiment shows that even for the narrow indices, differences exist between the Lick/IDS stars and other libraries (see Worthey & Ottaviani 1997; Sánchez-Blázquez et al. 2006a). The origin of these differences is not clear, but they need to be corrected.

Furthermore, the spectra of this library have a low effective S/N due to the significant flat-field noise (Dalle Ore et al. 1991; Worthey et al. 1994; Trager et al. 1998). This translates into larger random errors in the indices, much larger than in present-day galaxy data. It is worth noting that the accuracy of the measurements based on the Lick system is often limited by these transformations, rather than by the quality of the galaxy data.

4.1 A new line index system: LIS

With the advent of new stellar libraries, such as MILES, with better resolution, better S/N, larger number of stars and very complete coverage of the atmospheric parameter space, it is about time to revisit the standard spectrophotometric system at which the indices are measured. It is not our objective to tell the authors at which resolution the indices need to be measured. In fact, we recommend to use the flexibility provided by the model SSP SEDs and compare the measurements performed on each object with models with the same total broadening. However, this might not be a valid option in many cases, e.g. when a group of measurements is to be represented together in the same index–index diagram. It is also convenient to agree on a standard resolution at which to measure line strengths, so that measurements can be compared easily with previous studies and with colleagues, and to avoid systematic errors that might affect the conclusions. One of the reasons why the Lick/IDS system is still popular nowadays is because most previous studies have calculated their indices in this system. Although it is a good standard procedure to compare new measurements with previous works, the fact that those are transformed into the Lick/IDS systems perpetuates the problem. For this reason, we propose in this section a new line index system (LIS) with three new spectral resolutions at which to measure the Lick indices. Note that this new system should not be restricted to the Lick set of indices in a flux-calibrated system. In fact, LIS can be used for any index in the literature (e.g. for the Rose 1994 indices), including newly defined indices (e.g. Cervantes & Vazdekis 2009).

We provide conversions to transform the data from the Lick/IDS system to LIS as well as tables with index measurements in the new system for popular samples of Milky Way GCs, nearby elliptical galaxies and bulges. For this purpose, we use index tables already published by other authors and transform them into the new system. To calculate the conversion, we have broadened the MILES stars in common with the Lick/IDS library (218 stars in total) to the new standard resolutions defined for both GCs and galaxies and compare the indices measured in both data sets. Third-order polynomials were fitted in all cases. These transformations are given in Appendix A. In a forthcoming paper, we will present empirical fitting functions for the Lick indices at these new standard resolutions proposed here. A preliminary version of these fitting functions can be found in Martín-Hernández et al. (2007), which were computed at a resolution of 2.3 Å (FWHM). We concentrate here on the Lick/IDS suite of indices because it has been the most widely used in the literature.

The definition of this new system using the MILES stellar library has two main practical advantages as follows.

(i) The resolution of the MILES stars is constant as a function of wavelength. As a result, the user will not have to degrade the spectra with a wavelength-dependent function.

(ii) Additional offsets will not have to be applied to the data, as long as the measurements are flux calibrated (in a relative sense). Therefore, the system is universal and the index measurements are straightforward to perform.

It is very difficult to choose an appropriate resolution at which to define a new system, as it depends on the intrinsic broadening of the objects and the instrumental resolution. The Lick/IDS indices have been measured in a variety of objects, from GCs to giant elliptical galaxies, covering a very wide range in velocity dispersion and in data with a variety of instrumental resolutions. The appropriate resolution also depends on which indices are going to be measured; while some Lick/IDS indices do not change their sensitivity to age and metallicity with broadening, others (e.g. Ca4227, Fe4531) do. For these reasons, we consider it appropriate to define three different standard resolutions. The first one has been specifically chosen for stellar clusters and dwarf galaxy data, while the other two are more appropriate for working with massive galaxy spectra.

4.1.1 LIS-5.0 Å

When choosing a standard resolution at which to compare indices of GCs, we were guided by the resolution of existing high-quality GC data. Schiavon et al. (2005) presented a spectral library of 40 Galactic GCs with a resolution of ∼3.1 Å (FWHM). This represents an important comparison data base for extragalactic GC systems and a logical upper limit for our choice of resolution. However, the majority of extragalactic spectral data for GCs have lower resolution. Data from the Gemini/GMOS collaboration (e.g. Pierce et al. 2006a,b; Norris et al. 2008) exhibit a typical FWHM of ∼5 Å. Very similar to this are the Very Large Telescope/FORS spectra presented by Puzia et al. (2004). Keck/LRIS data from the SAGES[2] group have been generally taken at slightly higher resolutions of ∼2.8–4 Å (e.g. Strader et al. 2005; Beasley et al. 2006; Cenarro et al. 2007a; Chomiuk, Strader & Brodie 2008; Beasley et al. 2009). Since it

[2] http://www.ucolick.org/∼brodie/sages/sages/SAGES_Welcome.html

is considerably more straightforward to degrade higher resolution data to lower resolution than to attempt to correct lower resolution indices to higher resolution, we suggest using a resolution (FWHM) of 5 Å in GC index comparisons, a choice which encompasses all of the above data. This choice reflects a factor of 2 improvement in resolution over the Lick/IDS system.

Authors willing to compare their data with the models presented here will only have to broaden their spectra to a resolution of 5 Å (FWHM) (this corresponds to $\sigma = 127\,\mathrm{km\,s^{-1}}$ at 5000 Å) and measure the indices there. If they wish to compare with previous published data in the Lick/IDS system, then they can use the conversion provided in Table A1.

4.1.2 LIS-8.4 Å

For galaxies, we have decided to define two different standard resolutions. The first one, discussed in this subsection, is fixed at resolution FWHM = 8.4 Å (this corresponds to $\sigma = 214\,\mathrm{km\,s^{-1}}$ at 5000 Å). The reasons for this choice are twofold.

(i) It matches, roughly, the resolution of the Lick/IDS system in the Hβ–Mg triplet region. The indices in this region (e.g. Hβ, Mg*b*, Fe5270) are the most widely used in the literature and therefore the measurements in the new system will not differ considerably from previous measurements.

(ii) $200\,\mathrm{km\,s^{-1}}$ is roughly the mean velocity dispersion for the early-type galaxies in the Sloan Digital Sky Survey (SDSS; Bernardi et al. 2003a,b,c).

This system is particularly appropriate for studies of dwarf and intermediate-mass galaxies, where the total broadening of the spectra ($\sigma^2_{\mathrm{inst}} + \sigma^2_{\mathrm{gal}}$) is not higher than $\sigma = 214\,\mathrm{km\,s^{-1}}$ at 5000 Å. In this case, the author will only have to broaden their spectra to the proposed total σ using a Gaussian broadening function and to measure the indices.

If, on the contrary, the total broadening of the object is higher than this value, the author has the option of using the system LIS-14.0 Å or of correcting his/her measurements to a total broadening of 8.4 Å (FWHM) using polynomials (see e.g. Kuntschner 2000; Sánchez-Blázquez et al. 2006b).

In a similar way to LIS-5 Å, previous data in the Lick system can be converted into this new system using the polynomials given in Table A2.

4.1.3 LIS-14.0 Å.

The third system is defined at a resolution of FWHM = 14 Å (this corresponds to $\sigma = 357\,\mathrm{km\ s^{-1}}$ at 5000 Å). LIS-14.0 Å has been designed especially for the study of massive galaxies. In the spectra obtained for these galaxies, the broadening is dominated by the velocity dispersion of the stars. The total broadening is higher than the standard Lick/IDS resolution for which, in order to compare with the models, one usually had to perform a correction due to velocity dispersion of the galaxy. As mentioned above, this correction is one of the largest sources of systematic errors in the measurement of the indices (e.g. Kelson et al. 2006).

For studies that only analyse the stronger Lick indices in a sample of galaxies with velocity dispersions $\sigma > 200\,\mathrm{km\,s^{-1}}$, we suggest to broaden all the spectra by an amount such that the total resolution ($\sigma_{\mathrm{total}} = \sqrt{\sigma^2_{\mathrm{inst}} + \sigma^2_{\mathrm{gal}} + \sigma^2_{\mathrm{broad}}}$) matches FWHM = 14 Å, before measuring the indices, where σ_{inst} represents the instrumental resolution and σ_{gal} the velocity dispersion of the galaxy. This will help us to avoid performing any further correction to the indices due to broadening.

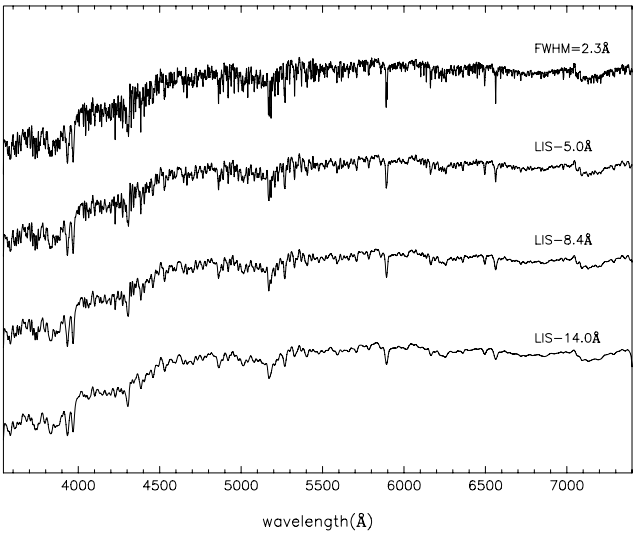

Figure 10. SSP SED of solar metallicity, 10 Gyr and Kroupa universal IMF, plotted for different resolutions. From top to bottom, FWHM = 2.3, 5.0, 8.4 and 14.0 Å. The latter three resolutions correspond to the new system of indices proposed here (LIS).

Fig. 10 shows the synthetic structure of an SSP with 10 Gyr and solar metallicity broadened to the resolution of the different LIS-systems. The polynomials required to transform the indices on the Lick/IDS system to this resolution are provided in Table A3.

4.2 Brief notes about system transformation

Most spectrographs keep the resolution constant in units of wavelength, rather than velocity. Therefore, the broadening of the spectra, if done in a linear wavelength scale, should be always performed using Gaussians of a fixed number of pixels. If the broadening of the data has to be made with a Gaussian with a constant width in $\mathrm{km\,s^{-1}}$, then the broadening in the spectra should be performed on a spectrum with a logarithmic wavelength scale.

It is common practice in studies of stellar populations to observe stars in common with the Lick/IDS library. This is done to derive offsets to transform the data on to the spectrophotometric system of the Lick library.[3] We stress here that this is necessary, *only* because the Lick/IDS spectra suffer from a number of calibration problems. However, these offsets will not correct properly any uncertainty in the calibration of the science spectra, as the position of the line index on the detector changes for extragalactic objects due to their redshift.

4.3 Reference tables

One of the reasons why many authors keep using the Lick/IDS system is to compare with previous studies, which are usually presented in this system. We provide here with a set of indices, obtained from several references already transformed to the new systems. The data are available at the CDS and in the electronic version of the paper (see Supporting Information).

[3] For most indices, the corrections are better described by linear relations instead of offsets; see the appendix in Sánchez-Blázquez et al. (2009).

We have selected several samples of early-type galaxies and GCs from the literature and transformed the line-strength indices to the new systems defined here. This is intended to provide a benchmark of indices properly transformed into LIS and measured on high quality data that other authors can use to compare with. The selected samples are as follows.

(i) Puzia et al. (2002) This sample comprises 12 Galactic GCs. Lick indices were measured from long-slit spectra obtained with the Boller & Chivens Spectrograph mounted on the 1.5 m telescope in La Silla. The wavelength coverage of the spectra ranges from 3400 to 7300 Å with a final resolution of ∼6.7 Å. All the spectra were observed with a slit width of 3.0 arcsec. We transformed the Lick indices into the new system using the transformations provided in this paper (Table A1).

(ii) Schiavon et al. (2005). This sample consists of 40 galactic GCs, obtained with the Blanco 4 m telescope at the Cerro Tololo Observatory. The spectra cover the range of ∼3350–6430 Å with 3.1 Å (FHWM) resolution. The S/N of the flux-calibrated spectra ranges from 50 to 240 Å^{-1} at 4000 Å and from 125 to 500 Å^{-1} at 5000 Å. The sample has been carefully selected to contain GCs with a range of ages and metallicities. The indices provided in Table 2 have been measured directly in the spectra degraded to the LIS-5.0 Å resolution.

(iii) Trager et al. (2000). This sample consists of 40 galaxies drawn from that of González (1993) intended to cover, relatively uniformly, the full range of velocity dispersion, line strength and colour displayed by local elliptical galaxies. The line-strength indices (i.e. Hβ, Mg*b*, Fe5270, Fe5335) were measured from long-slit data obtained with the CCD Cassegrain Spectrograph on the 3 m Shane Telescope of Lick Observatory. The spectral features were measured within r_e/8 aperture. The indices were transformed into the new system applying the transformations from Tables A2 and A3.

(iv) Sánchez-Blázquez et al. (2006b). This sample consists of 98 early-type galaxies including ellipticals and lenticulars, spanning a wide range in central velocity dispersion (σ). The sample contains galaxies in different environments, such as isolated galaxies and galaxies in groups, and in several clusters. The central spectra were extracted within an aperture of 0.6 kpc (assuming $H_0 = 70\,\mathrm{km\,s^{-1}}$). The spectra were corrected from the presence of nebular emission using GANDALF (Sarzi et al. 2006), instead of using the [O III]λ-based correction published in the original paper. We use the models provided in this paper as templates. The spectral range covers from ∼3500/3700 (depending on the run) to ∼5200/5700 Å, with spectral resolution ranging from 3.6 to 6.56 Å (FWHM) (see the original paper for more details). The indices provided in Table 2 have been measured in the emission-free spectra previously degraded at the different LIS resolutions. For those galaxies with a σ larger than the LIS resolution an additive correction was made using the kinematic templates [the combination of SSP models that better reproduced the galaxy spectra obtained in the measurement of σ using PPXF (Cappellari & Emsellem 2004)], following the prescriptions in Kelson et al. (2006). The correction was obtained as the difference in the indices measured in these templates degraded at the LIS resolution and at $\sqrt{\sigma_{\rm gal}^2 + \sigma_{\rm ins}^2}$, where $\sigma_{\rm gal}$ is the velocity dispersion of the galaxy and $\sigma_{\rm inst}$ the instrumental resolution.

(v) Yamada et al. (2006). This sample consists of 14 galaxies, morphologically classified as E in the Virgo cluster. The galaxies were selected with three criteria as follows: (1) they had to be classified as an elliptical galaxy in the RC3 catalogue (de Vaucouleurs et al. 1991), (2) they had to be free from strong emission lines and (3) they had to cover a wide range of luminosity evenly distributed along the colour–magnitude of the Virgo cluster. These extremely high quality spectra, which have been extracted within an aperture of r_e/10, have an S/N well above >100 Å^{-1} for all the galaxies and about ∼500 Å^{-1} for some of them. The spectra cover a wavelength range from 3800 to 5800 Å and the resolution ranges from 2.0 to 3.1 Å, depending on the observational runs, which have been performed at the William Herschel Telescope (WHT; 4.2 m) and Subaru telescope (8.2 m). For full details of the sample, we refer the reader to the original paper. Three galaxies have a velocity dispersion larger than the resolution of the LIS-8.4 Å and the indices in this system were corrected in the same way as in the Sánchez-Blázquez et al. (2006b) sample.

(vi) Kuntschner et al. (2006). This sample consists of 48 E/S0 galaxies in the Spectrographic Areal Unit for Research on Optical Nebulae (SAURON) survey of early-type galaxies (de Zeeuw et al. 2002) at the William Herschel 4.2 m telescope in La Palma. We use here the line-strength measurements (i.e. Hβ, Fe5015, Mg*b*) averaged within the r_e/8 aperture. The spectral coverage of the observed SAURON integral-field observations ranges from 4800 to 5380 Å at a resolution of ∼4.2 Å (FWHM). The indices of Table 2 were obtained by applying the transformations of Tables A2 and A3 to the indices transformed into the Lick systems provided in the original paper.

Table 2 shows a portion of the tables that illustrate its format and content. The table contains the Lick/IDS indices measured at the different LIS resolutions with the index definitions provided in Trager et al. (1998). The full tables are available in the electronic version of the paper (see Supporting Information).

Fig. 11 shows the commonly used index–index diagnostic diagram Hβ versus [MgFe] in the new LIS-5.0 Å system for the Puzia et al. (2002) and Schiavon et al. (2005) GC samples. We use the indices in Table 2. Note that we do not plot the model indices for SSPs younger than 10 Gyr for [M/H] = −2.3, according to our Q_n parameter analysis. In Figs 12 and 13, we show the Hβ versus [MgFe] and Hβ versus [MgFe50] diagrams for the four galaxy samples in both LIS-8.4 Å and LIS-14.0 Å. Note that for all the galaxies of Kuntschner et al. (2006) and for 36 galaxies in the Sánchez-Blázquez et al. (2006b) sample it was not possible to plot the [MgFe] index, as either one or the two iron indices (Fe5270, Fe5335) required to calculate this index were outside the covered spectral range. Note that we used GANDALF (Sarzi et al. 2006) to remove nebular emission from the galaxy spectra of Sánchez-Blázquez et al. (2006b) and Yamada et al. (2006). We refer the reader to all these original works for a detailed discussion of the results obtained.

4.4 MILES SSP SED index measurements

Fig. 14 shows the predicted time evolution of our solar metallicity and Salpeter IMF models for a selection of line-strength indices measured at four different spectral resolutions: the nominal resolution of the models, i.e. FWHM = 2.3 Å, and the resolutions of LIS-5.0 Å, LIS-8.4 Å and LIS-14.0 Å (i.e. FWHM = 5, 8.4 and 14 Å, respectively). It can be seen that the sensitivity of some indices to variations in resolution is barely noticeable. This is the case for the wide molecular index definitions, i.e. CN, Mg and TiO. For some lines, however, broadening the spectra means losing part of the information contained in them (e.g. Ca4227). The most critical situation when analysing data by means of diagnostic diagrams based on these indices happens when the relative variation of the index with age depends on the resolution. Authors should keep this in mind in order to choose the right system and diagnostics to work with

Table 2. Lick indices measured in the LIS for GCs and galaxies from selected references.

	Puzia et al. (2002) [LIS-5.0 Å]																							
Name	$H\delta_A$	$H\delta_F$	CN_1	CN_2	Ca4227	G4300	$H\gamma_A$	$H\gamma_F$	Fe4383	Ca4455	Fe4531	C4668	$H\beta$	Fe5015	Mg_1	Mg_2	Mgb	Fe5270	Fe5335	Fe5406	Fe5709	Fe5782	Na5895	TiO_1	TiO_2
NGC 5927	−2.2576	0.1134	0.0975	0.1362	0.8685	4.9847	−4.1324	−1.2751	2.9922	0.6743	2.6763	3.0431	1.7502	4.9167	0.0756	0.1999	3.5827	2.2866	2.0628	1.3108	0.5205	0.8942	4.4516	0.0377	0.0895
	0.0388	0.0269	0.0009	0.0012	0.0176	0.0282	0.0408	0.0277	0.0493	0.0247	0.0424	0.0629	0.0335	0.0715	0.0007	0.0009	0.0358	0.0442	0.0524	0.0381	0.0340	0.0317	0.0396	0.0008	0.0008
NGC 6218	3.1849	2.8266	−0.0543	−0.0298	0.2969	3.3555	1.4944	1.9157	0.1026	0.0319	1.3028	0.1446	2.8334	2.8312	0.0232	0.0582	1.1352	0.8644	1.0777	0.4432	−0.1952	0.2400	1.1520	0.0101	0.0045
	0.0186	0.0123	0.0007	0.0007	0.0098	0.0251	0.0248	0.0161	0.0358	0.0127	0.0344	0.0535	0.0278	0.0691	0.0006	0.0008	0.0343	0.0311	0.0490	0.0289	0.0345	0.0275	0.0387	0.0009	0.0010
NGC 6284	2.0326	2.6239	−0.0210	0.0056	0.3717	3.8327	0.2104	1.3103	0.8237	0.1649	1.8133	0.5586	2.5439	3.2827	0.0375	0.0854	1.5008	0.9413	1.2086	0.6797	0.1218	0.3272	2.2529	0.0083	0.0044
	0.0250	0.0187	0.0007	0.0008	0.0128	0.0248	0.0288	0.0207	0.0442	0.0161	0.0363	0.0575	0.0272	0.0752	0.0007	0.0009	0.0323	0.0364	0.0454	0.0328	0.0350	0.0227	0.0420	0.0008	0.0008
NGC 6356	−1.0805	0.6216	0.0606	0.0891	0.6710	5.4774	−3.8769	−0.9782	2.3657	0.4230	2.6000	1.7702	1.7484	4.1852	0.0647	0.1602	2.8145	1.7640	1.8961	1.0925	0.4241	0.5489	3.1437	0.0224	0.0502
	0.0186	0.0117	0.0006	0.0007	0.0100	0.0142	0.0214	0.0139	0.0272	0.0122	0.0253	0.0440	0.0189	0.0446	0.0005	0.0006	0.0214	0.0231	0.0326	0.0210	0.0217	0.0191	0.0262	0.0005	0.0006
NGC 6388	−0.2366	1.0513	0.0602	0.0917	0.5320	4.8704	−2.6754	−0.1589	2.4337	0.3673	2.5714	1.7768	2.1259	4.2186	0.0502	0.1310	2.1997	1.9315	1.9042	1.1532	0.5123	0.6698	3.6860	0.0219	0.0447
	0.0100	0.0062	0.0003	0.0004	0.0049	0.0092	0.0128	0.0078	0.0158	0.0066	0.0120	0.0196	0.0098	0.0244	0.0002	0.0003	0.0107	0.0158	0.0146	0.0125	0.0106	0.0096	0.0143	0.0003	0.0003
NGC 6441	−0.2459	1.1013	0.0682	0.0997	0.6307	4.8525	−2.8379	−0.1968	2.7413	0.3912	2.6228	1.7832	2.0552	4.3328	0.0640	0.1586	2.7556	2.0015	1.9567	1.1619	0.5665	0.8016	3.9727	0.0128	0.0513
	0.0260	0.0176	0.0007	0.0009	0.0150	0.0237	0.0271	0.0200	0.0333	0.0157	0.0320	0.0501	0.0240	0.0591	0.0006	0.0007	0.0269	0.0379	0.0432	0.0253	0.0258	0.0239	0.0265	0.0006	0.0006
NGC 6528	−2.0478	0.3512	0.1078	0.1389	1.0559	5.6030	−5.6367	−1.6013	4.6496	0.7368	2.9746	4.4146	1.8889	5.2490	0.1033	0.2382	3.7516	2.4408	2.5976	1.7286	0.8399	0.8249	5.1220	0.0575	0.1196
	0.0439	0.0294	0.0011	0.0013	0.0194	0.0303	0.0452	0.0302	0.0509	0.0276	0.0447	0.0796	0.0351	0.0807	0.0009	0.0009	0.0395	0.0457	0.0479	0.0476	0.0311	0.0364	0.0402	0.0010	0.0009
NGC 6553	−2.2176	0.8167	0.1465	0.1810	1.2451	5.7732	−5.8327	−1.6070	3.9143	0.6909	3.3030	3.7248	2.0026	5.7870	0.0897	0.2324	3.9036	2.7011	2.5835	1.3858	0.7923	1.1831	3.7845	0.0523	0.1340
	0.0705	0.0432	0.0017	0.0022	0.0328	0.0476	0.0639	0.0425	0.0777	0.0460	0.0672	0.1140	0.0521	0.0971	0.0011	0.0013	0.0514	0.0702	0.0753	0.0521	0.0424	0.0454	0.0563	0.0010	0.0009
NGC 6624	−0.9553	0.6427	0.0650	0.0977	0.6539	5.3411	−3.7187	−0.8093	2.4164	0.4004	2.5801	1.8939	1.7645	4.3141	0.0628	0.1554	2.7574	1.8628	1.8745	1.1159	0.5191	0.6466	2.5670	0.0337	0.0593
	0.0184	0.0136	0.0005	0.0006	0.0092	0.0144	0.0209	0.0161	0.0252	0.0128	0.0218	0.0366	0.0199	0.0422	0.0004	0.0005	0.0166	0.0243	0.0342	0.0256	0.0173	0.0214	0.0219	0.0005	0.0005
NGC 6626	2.3537	2.4215	−0.0247	0.0026	0.3655	3.7828	0.1746	1.2743	0.7371	0.0931	1.6467	0.6247	2.3904	3.3106	0.0364	0.0811	1.4305	1.1532	1.1603	0.7001	0.1977	0.4725	1.9530	0.0187	0.0363
	0.0222	0.0178	0.0006	0.0009	0.0113	0.0260	0.0278	0.0171	0.0381	0.0124	0.0351	0.0571	0.0278	0.0669	0.0005	0.0006	0.0299	0.0322	0.0365	0.0272	0.0304	0.0269	0.0322	0.0007	0.0006
NGC 6637	−1.1022	0.3993	0.0417	0.0691	0.5761	5.5794	−3.9200	−1.0808	2.1029	0.3539	2.4863	1.7632	1.7367	4.0857	0.0501	0.1388	2.5752	1.6781	1.6068	0.9602	0.3732	0.4894	2.4638	0.0263	0.0418
	0.0155	0.0107	0.0004	0.0005	0.0071	0.0105	0.0175	0.0127	0.0214	0.0096	0.0200	0.0303	0.0141	0.0365	0.0004	0.0005	0.0164	0.0212	0.0237	0.0170	0.0143	0.0144	0.0225	0.0004	0.0005
NGC 6981	1.5589	1.7715	−0.0262	−0.0091	0.3862	3.5881	0.4667	1.2872	0.1925	0.0895	1.3977	0.3620	2.5091	2.7705	0.0265	0.0532	1.1555	0.9544	0.7882	0.3914	−0.1326	0.1239	1.2737	0.0070	−0.0034
	0.0179	0.0127	0.0006	0.0007	0.0091	0.0208	0.0220	0.0164	0.0360	0.0126	0.0333	0.0475	0.0255	0.0619	0.0006	0.0007	0.0304	0.0323	0.0394	0.0218	0.0333	0.0151	0.0367	0.0006	0.0008

The complete version of this table can be found in the electronic version of the journal – see Supporting Information.

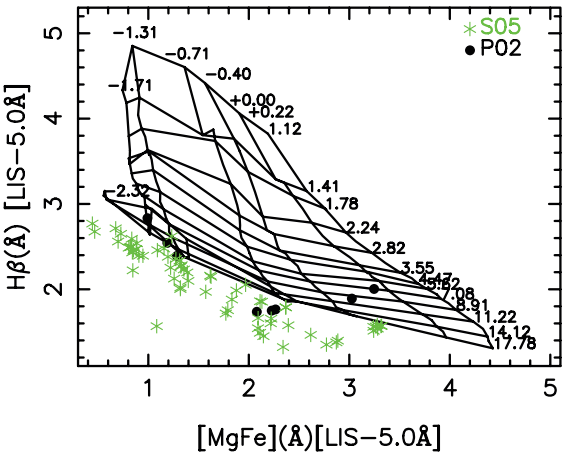

Figure 11. Hβ versus [MgFe] diagnostic diagram in the LIS-5.0 Å system. Asterisks represent the GC sample of Schiavon et al. (2005), whereas the solid circles represent the clusters of Puzia et al. (2002). We used the indices listed in Table 2 (the electronic version). For the models, we used a Kroupa universal IMF.

the data. Our recommendation is to use the most straightforward approach possible, which is to work with the model SEDs smoothed to match the total resolution of the data. This approach allows the user to take full advantage of the whole information contained in the data (see V99 for an extensive discussion). Interestingly, we note that the time evolution for most Lick indices shows a minimum for intermediate-age stellar populations in the range of 0.1–1.0 Gyr, as already mentioned in Section 3.1. This is particularly evident for the CN indices.

Fig. 15 is similar to Fig. 14, but here several Balmer index definitions are shown. We plot the standard Lick Hβ index and the four higher order Balmer indices of Worthey & Ottaviani (1997). We also include two of the age indicators of Vazdekis & Arimoto (1999), the recently defined Hβ_o index of Cervantes & Vazdekis (2009) and the D4000 break (e.g. Gorgas et al. 1999). We see that for all the Balmer index definitions, the dependence on resolution is marginal or virtually nil (e.g. the 4000 Å break). The two Hγ_σ of Vazdekis & Arimoto (1999) are specifically defined to be insensitive to resolution. For this reason we only plot for Hγ_{125} the values corresponding to the resolution of LIS-5.0 Å and for Hγ_{200} the values corresponding to the resolution of LIS-8.4 Å as these

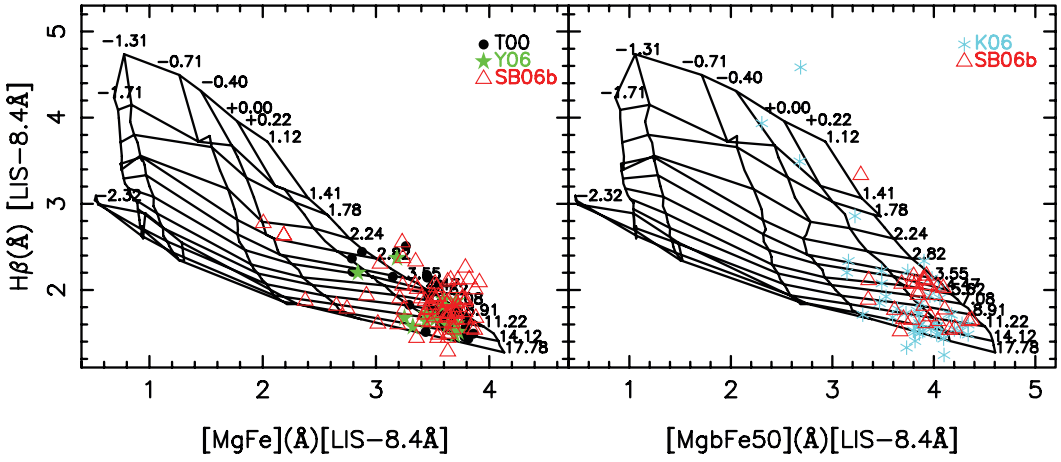

Figure 12. Hβ versus [MgFe] and Hβ versus [MgFe50] diagnostics diagrams in LIS-8.4 Å. In the left-hand panel, we plot the galaxy samples of Trager et al. (2000) (solid circles), Yamada et al. (2006) (stars) and Sánchez-Blázquez et al. (2006b) (open triangles). In the right-hand panel, we plot the galaxy sample of Kuntschner et al. (2006) (asterisks) and 36 galaxies from the sample of Sánchez-Blázquez et al. (2006b) (open triangles), as for all these galaxies the two iron lines required to calculate the [MgFe] index fall outside the covered spectral range (i.e. Fe5270 and Fe5335).

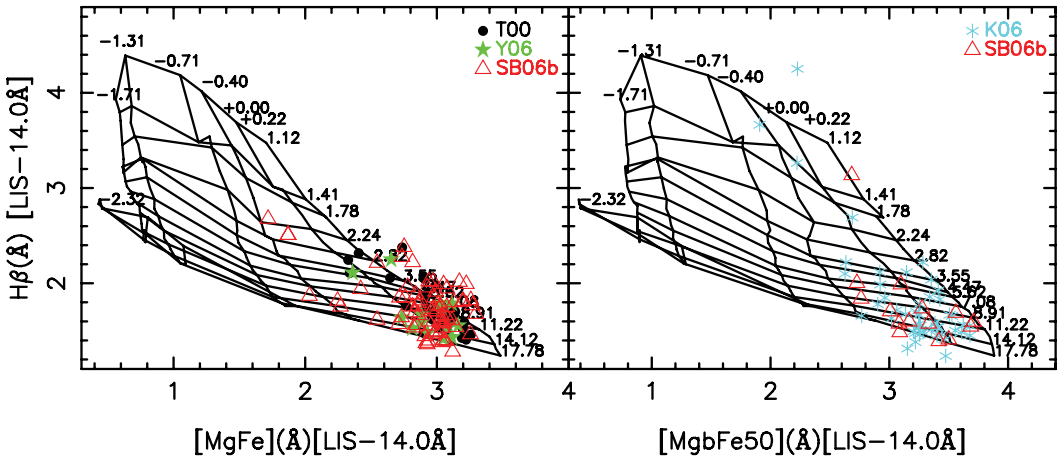

Figure 13. Same as in Fig. 12 but for LIS-14.0 Å.

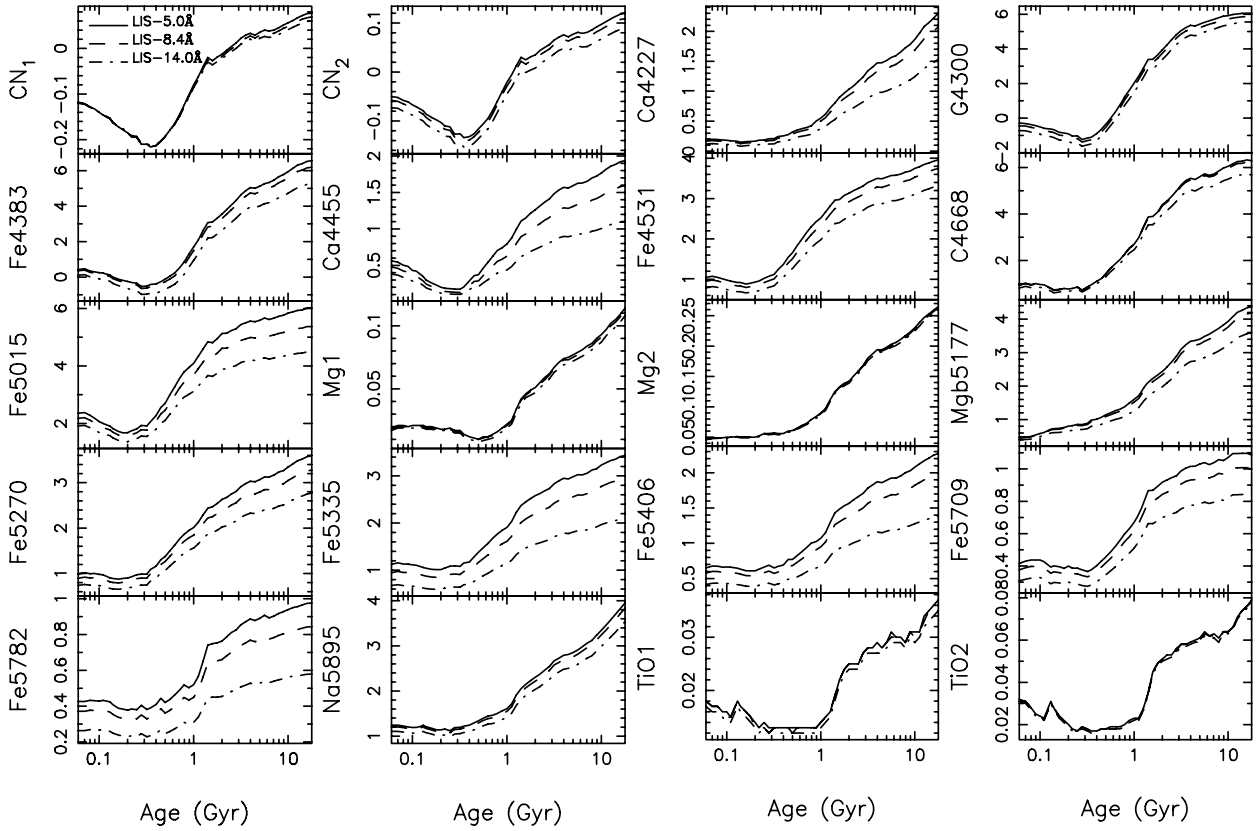

Figure 14. Time evolution of several Lick line-strength indices measured on our new SSP SEDs for solar metallicity and Kroupa universal IMF, smoothed to different resolutions. Solid line: resolution of LIS-5.0 Å (FWHM = 5 Å); dashed line: resolution of LIS-8.4 Å (FHWM = 8.4 Å); dash–dotted line: resolution of LIS-14.0 Å (FWHM = 14 Å).

two resolutions fall within the stability range of these indices, respectively. We did not include the third index defined in Vazdekis & Arimoto (1999), $H\gamma_{275}$, as the resolution of LIS-14.0 Å is larger than is allowed for this index. Interestingly, being almost negligible, we see that whereas the sensitivity to resolution for the new $H\beta_o$ index is slightly larger than that for the standard $H\beta$ Lick index for old stellar populations, the situation is reverse for ages smaller than ∼1 Gyr. The higher order Balmer line index definitions of Worthey & Ottaviani (1997) also show higher resolution sensitivity for younger stellar populations. Note that all Balmer indices, except the D4000 break, peak at ∼0.3 Gyr and therefore the fits obtained on the basis of these indices can have two solutions. Kauffmann et al. (2003) take advantage of the behaviour of these indices to define diagnostics for constraining the star formation history.

Figs 16 and 17 show the variation of the line-strength indices as a function of metallicity predicted by our new models for stellar populations of 10 Gyr and the Salpeter IMF. As in the previous figures, the predictions are shown for three different resolutions: FWHM = 5.0, 8.4 and 14 Å , respectively. We see a resolution-dependent differential behaviour as a function of metallicity for several indices, such as Ca4227, Fe5335 and Fe5782. This shows that a lot of care has to be taken to match the resolution of data and models when comparing both as, otherwise, artificial trends can be derived (see Kelson et al. 2006). Fig. 17 shows the somewhat opposite dependence on the resolution of two $H\beta$ index definitions: $H\beta_o$ shows larger resolution dependence than $H\beta$ for higher metallicities. Note, however, the insensitivity to metallicity achieved by this $H\beta_o$ definition for [M/H] > −1, which is not seen for the commonly used $H\beta$ Lick index. Such insensitivity is also shown by the two $H\gamma$ indices of Vazdekis & Arimoto (1999) plotted here. We are not describing here in detail the index behaviour as a function of metallicity and age, but the metallicity insensitivity of the two TiO molecular indices for [M/H] > −0.5 is particularly noteworthy.

4.5 $H\beta$: comparison with the fitting function predictions

In Fig. 18 we focus specifically on the behaviour of the most popular age indicator, the Lick $H\beta$ index, as a function of age (plotted in a linear scale, for ages of >1 Gyr) and metallicity. In this figure we compare the index computed on the basis of the empirical fitting functions of Worthey et al. (1994), using the Vazdekis et al. (1996) code, as updated in this work and transformed to the LIS-8.4 Å system following Table A2, with the $H\beta$ index measured on the SSP SEDs, once smoothed to the LIS-8.4 Å resolution. We see that the models based on MILES provide larger values for solar and super-solar metallicities and for [M/H] < −1 than those based on the Lick/IDS fitting functions. This implies that when using MILES models, the ages obtained are older by about ∼2 Gyr for SSPs around ∼10 Gyr.

Another interesting effect at metallicities [M/H] < −1 is that, for ages above ∼12 Gyr, $H\beta$ starts increasing instead of decreasing as expected. This effect, not seen at higher metallicities, is attributed to the contributions of the horizontal branch (HB) stars (e.g. Maraston & Thomas 2000). Therefore the $H\beta$ index, rather than indicating the age of the stellar population due to its sensitivity to the $T_{\rm eff}$ of the turnoff stars, becomes sensitive to the HB morphology. This result is in agreement with Maraston & Thomas (2000). We see, however, that this sudden increase in the strength of the $H\beta$ index is

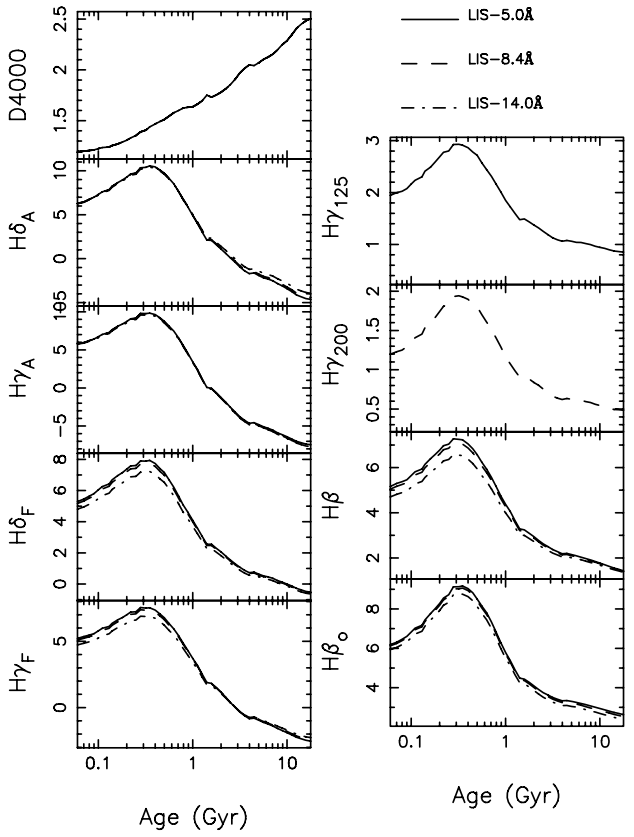

Figure 15. Time evolution of various Balmer line-strength indices measured on the SSP SEDs of solar metallicity and Kroupa universal IMF smoothed at different resolutions as in Fig. 14.

less visible for the new predictions for the three lowest metallicities plotted in this figure. In fact, the effect virtually disappears for [M/H] < -2. This result would have important implications for the interpretation of integrated spectra of composite stellar systems, for which the Balmer lines, such as the Hβ index, are the primary age diagnostics. In fact, Maraston & Thomas (2000) have suggested that a spread in the metallicity of an old stellar population can account for most of the dispersion of Hβ values observed in the family of ellipticals – due to the higher Hβ index of the metal-poor stars – without the need of a young population as had been previously suggested in other studies (e.g. González 1993). As we obtain with MILES higher Hβ strengths, the required fraction for the metal-poor component should be smaller than is suggested by Maraston & Thomas (2000).

It is very important to note that in Fig. 18, we are comparing the same synthesis code with identical HB prescriptions. The different behaviour at low metallicities between the two sets of predictions should be fully attributed therefore to the limitations of the Lick stellar library, as it becomes evident when comparing the Q_n values obtained for these two sets of predictions in this low metallicity regime (see the second panel of Fig. 6 and the left-hand panel of Fig. 7).[4]

[4] In fact, guided by the Q_n parameter obtained, we only plotted the Hβ values for ages larger than 10 Gyr for the MILES models of [M/H] $= -2.3$. However we plotted the Hβ values obtained for the Lick/IDS fitting functions for [M/H] $= -1.7$, despite the fact that their corresponding Q_n values are lower than 1 (see the left-hand panel of Fig. 7).

5 MILES SSP COLOURS

One of the main advantages of MILES is that the stellar spectra were carefully flux-calibrated. In fact, we obtained for each star of the library a wide-slit spectrum to avoid selective flux losses due to the differential refraction effect (see SB06a for details). This allows us to measure accurate colours from the synthesized SSP SEDs. This is performed by convolving the SED with the corresponding filter responses. To obtain the Johnson $B - V$ broad-band colour we use the filters of Buser & Kurucz (1978), with the zero-points set with Vega. To obtain the zero-point for the B and V filters, we used two different Vega SEDs from Hayes (1985) and Bohlin & Gilliland (2004), the latter based on high S/N Space Telescope Imaging Spectrograph (STIS) observations and extrapolated to higher wavelengths using Kurucz model atmospheres. After normalizing the synthetic spectra to the SED of Vega, we measured the $B - V$ colours by applying the selected filter transmission curves.

The results are shown in Fig. 19. We also plot, for comparison, the photometric version of this colour following Vazdekis et al. (1996) which is computed with the Alonso et al. (1996, 1999) calibrations. The figure shows a good agreement for nearly all ages and metallicities, within the typical photometric uncertainties derived from the zero-point of the B and V filters, as shown by the colour differences using two different normalizations of the Vega spectrum. We obtain rather similar time evolution colour curves for all the metallicities, with an offset of $\sim$0.02 mag. For the SSPs with [M/H] $= -2.32$ the offset can be as large as $\sim$0.05 mag (MILES SED colours slightly bluer), which is well below the photometric errors of the colours. Note, however, that for this metallicity the MILES models are barely acceptable, as shown by the Q parameter (see Fig. 6). This is because of the stellar parameter coverage of the MILES library and the fact that colour transformation is not accurate at such low metallicity.

A rather similar offset ($\sim$0.015 mag) has been quoted in SB06a (see their fig. 8) by comparing the $B - V$ colours derived from MILES stellar spectra to the values tabulated in the Lausanne photometric data base (Mermilliod, Mermilliod & Hauck 1997) for the same stars. As discussed in SB06a, this offset sets an upper limit to the systematic uncertainties of our photometry. For the sake of clarity, we do not show in Fig. 19 the colours obtained from the model SEDs computed with the temperature scale of González-Hernández & Bonifacio (2009). These models provide a redder $B - V$ colour by $\sim$0.02 mag, i.e. similar to the zero-point uncertainties. This is because for a given temperature, the stellar population model selects cooler spectra as the González-Hernández & Bonifacio (2009) temperatures are hotter than MILES by 51 K.

The results presented here show that the colours derived from our models, either those predicted via photometric libraries or the ones measured from our MILES SSP SEDs, are consistent. Such agreement shows the reliability of the temperatures adopted in C07a, which are consistent with the temperature scales of Alonso et al. (1996, 1999), i.e. the photometric libraries that feed our models. We also provide, in an electronic form and on the web (see Section 7), colours measured directly in the MILES spectra using combinations of various filter systems that are commonly used in the literature [e.g. SDSS, *Hubble Space Telescope* (*HST*)].

6 APPLICATIONS TO STELLAR CLUSTER AND GALAXY DATA

We compare, in this section, our new model SEDs with a set of representative stellar clusters of varying ages and metallicities. We

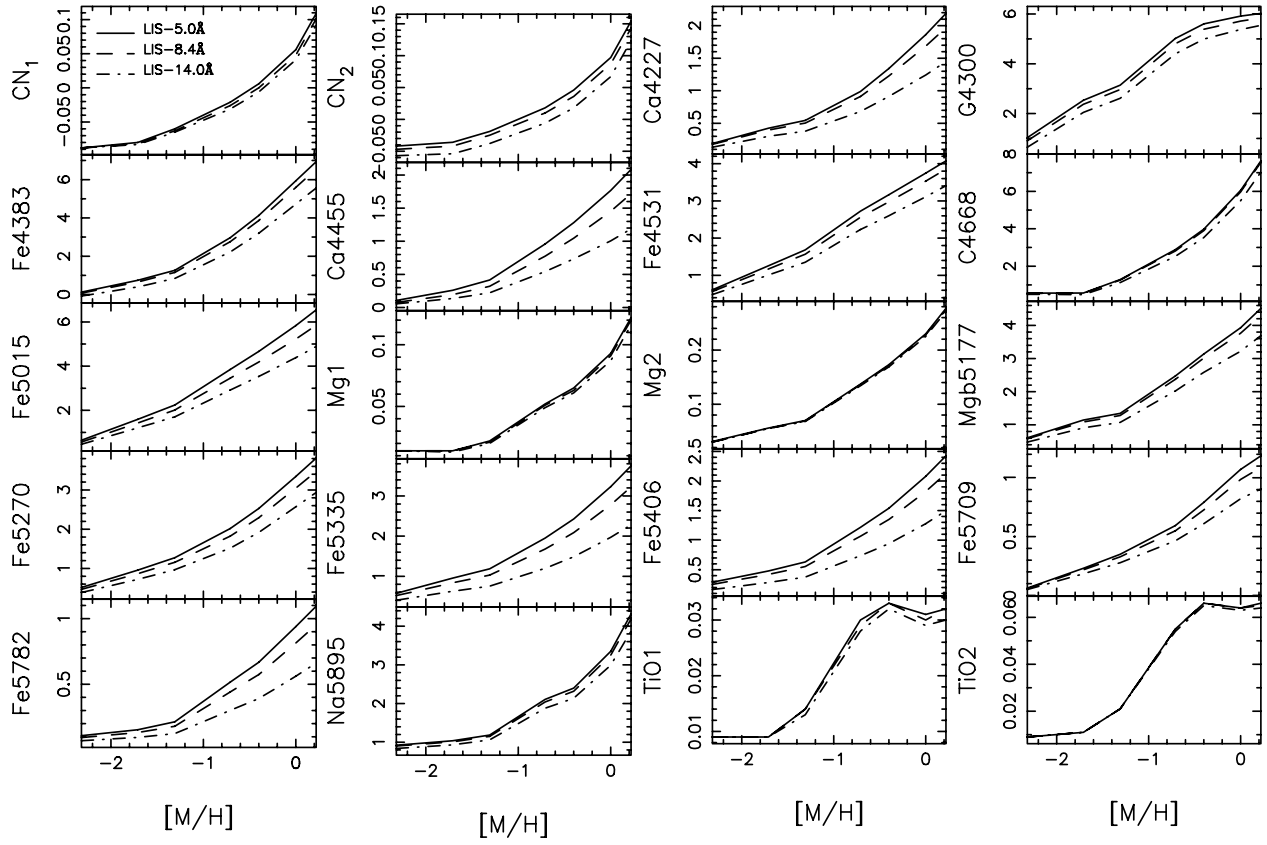

Figure 16. Variation of line-strength indices with metallicity predicted by our single stellar population models of 10 Gyr and Kroupa universal IMF. Different line styles show predictions for indices measured at different spectral resolutions, as in Fig. 14.

also illustrate the use and capabilities of these models for the study of galaxies with varying ages, metallicities, abundance ratios and masses, by giving a few examples for some well-studied galaxies.

6.1 Stellar clusters

Galactic GCs allow us to uniquely test our evolutionary synthesis models, since independent age and metallicity estimates are available through deep colour–magnitude diagram (CMD) analyses. These studies have concluded that, in most cases, GCs can be considered as formed in a single burst, which is characterized by a single age and a single metallicity, i.e. an SSP. Note, however, that there are clusters for which two stellar components have been identified (e.g. Meylan 2003) and that stochastic effects (e.g. Cerviño et al. 2002) may affect significantly their integrated spectra.

We have selected three representative Galactic GCs, with varying metallicities, from the sample of Schiavon et al. (2005), which is composed of 40 clusters. These authors obtained integrated spectra of a high S/N (∼250) covering the range λλ3350–6430 Å with 3.1 Å (FHWM) resolution. Fig. 20 shows the spectra and the best SSP SED fits overplotted. We used, for this purpose, our SSP SED library with the Kroupa universal IMF. The SSP SEDs were conveniently smoothed to match the instrumental resolution of the observations (i.e. $\sigma \sim 120\,\mathrm{km\,s^{-1}}$). We normalized the stellar cluster spectra and the model SEDs at 5000 Å, but we did not modify the spectral shape of the data (and the models) to perform the fits. The best fit is understood as the one that minimizes the residuals, which are also plotted in the figure at the same scale. The ages and metallicities obtained fully agree with the CMD-derived estimates of the Harris (1996) catalogue. For 47 Tuc, we obtained the same fit as in V99. For NGC 5904 we derived a younger age, in agreement with the very deep CMD study of Marin-Franch et al. (2009) who have estimated for this cluster a relative age of 0.83, i.e. the cluster is located within their young GC branch. We also found a younger age for this cluster, by means of a line-strength analysis that included the newly defined $H\beta_o$ age indicator of Cervantes & Vazdekis (2009). The higher $H\beta$ value obtained for this cluster is attributed in part to the presence of an increased fraction of blue stragglers (see Cenarro et al. 2008).

The residuals of Fig. 20 do not show any significant colour difference in the covered spectral range, but some very low-frequency variations that can be fully attributed to differences in the flux calibration. In fact, note that these low-frequency residuals are qualitatively identical among the three clusters. However the residuals show differences in various molecular bands, mainly in the blue part of the spectra for all the clusters. In particular, CN features at ∼3860 and ∼4150 Å are much stronger in the clusters than in the models. We also see a residual in the *G* band at ∼4300 Å, this absorption being weaker in the data. The CN-strong absorption, and its anticorrelation with CH, is a well-known feature in the Galactic GC family, which has been shown in both its individual stars (e.g. Norris & Freeman 1979) and its integrated spectra (e.g. Rose & Tripicco 1986). A similar result is obtained in V99 for 47 Tuc, but using a different input stellar spectral library and also a different spectrum for the cluster. Such a CN-strong absorption feature has also been reported for extragalactic GCs, such as NGC 1407 (Cenarro et al. 2007b). Their Lick/IDS $C_2$4668 versus CN_2 diagram shows the same anticorrelation with respect to the scaled-solar abundance ratios. Overall, we find that the residuals bluewards

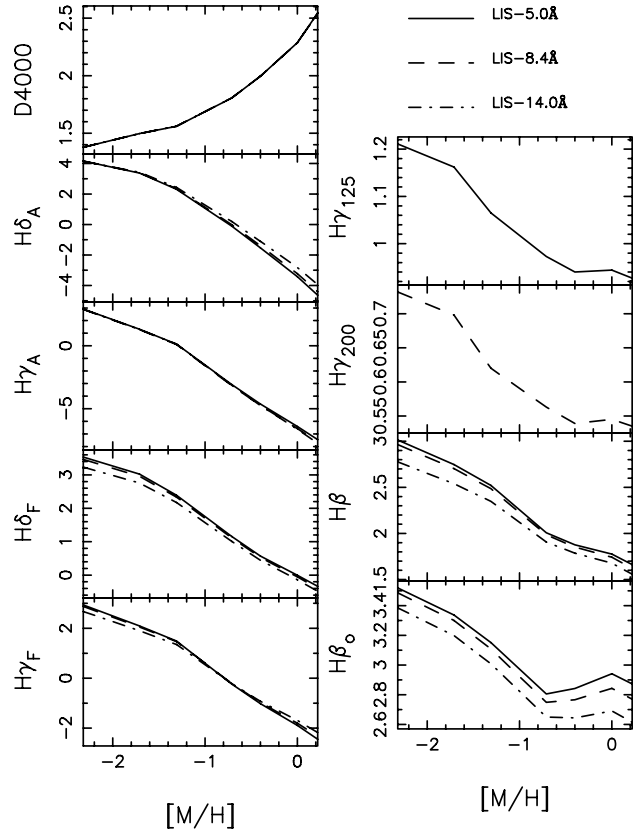

Figure 17. Variation of Balmer line-strength indices with metallicity predicted by our single stellar population models of 10 Gyr and Kroupa universal IMF. Different line styles show predictions for indices measured at different spectral resolutions, as in Fig. 14.

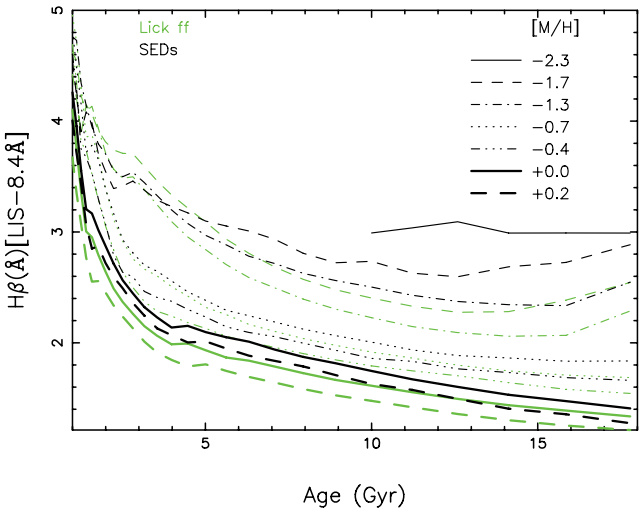

Figure 18. Comparison of the Hβ index computed on the basis of the empirical fitting functions of Worthey et al. (1994), using the models of Vazdekis et al. (1996), as updated in this work and transformed to the LIS-8.4 Å system following Table A2, with the index measured on the SSP SEDs, once smoothed to the LIS-8.4 Å resolution. For the lowest metallicity, we only plot the results for SSPs older than 10 Gyr according to our qualitative analysis shown in the second panel of Fig. 6. However, for the sake of the discussion we also show the predictions based on the Lick/IDS fitting functions for [M/H] = −1.7, even though we do not consider them to be of good quality because of the low number of stars at those metallicities.

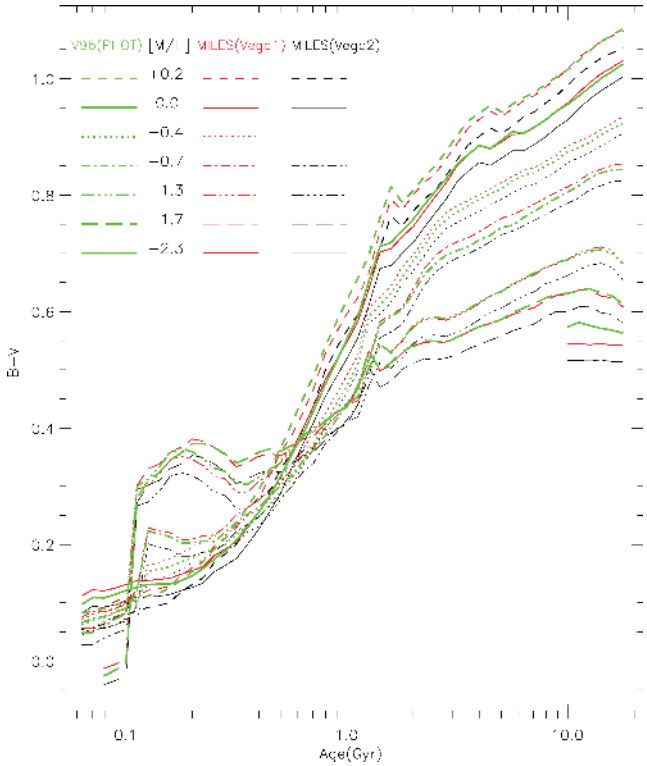

Figure 19. We plot the broad-band $B - V$ colour derived from the SSP SEDs for different ages and metallicities (as indicated within the panel) and the Kroupa universal IMF with the zero-point set with two different Vega spectra in black (very thin) and red (thicker) (see the text for details). The thickest green line represents the photometric colour computed by Vazdekis et al. (1996), as updated in this work, which is based on extensive empirical photometric stellar libraries.

of ∼4300 Å are significantly larger than for the redder part of the spectra for all the clusters. We do not discard possible effects due to the fact that the Milky Way GCs show oxygen-enhanced abundance ratios for low metallicities. In fact, Cassisi et al. (2004) have shown that such effects become relevant for the spectral ranges covered by the B, and mostly U, broad-band filters. Therefore, an appropriate modelling for these clusters requires working with such α-enhanced stellar evolutionary isochrones as well as the use of stellar spectra with a similar abundance pattern. In addition, we also require to use specific stellar spectra with CN-strong absorption features and CN-enhanced isochrones.

In Fig. 21, we show our SED fit to the integrated spectrum of the standard open cluster M67 (Schiavon, Caldwell & Rose 2004). Unlike for the GCs of Fig. 20, these authors obtained the integrated spectrum for M67 by co-adding individual spectra of cluster members, weighted according to their luminosities and relative numbers. The age and metallicity obtained are in good agreement with these authors (see also Schiavon 2007) and with our isochrone fitting results (Vazdekis et al. 1996) within the uncertainties. The residuals only show a low-frequency pattern, which is related to differences in the flux calibration. However, the higher frequency residuals are negligible. It is particularly interesting that, unlike in Fig. 20, we do not see the residuals bluewards of 4300 Å. This shows that all relevant spectral types are present in the MILES library. Therefore, the residuals obtained for Galactic GCs can be attributed to the non-solar abundance ratios present in these clusters. However, we

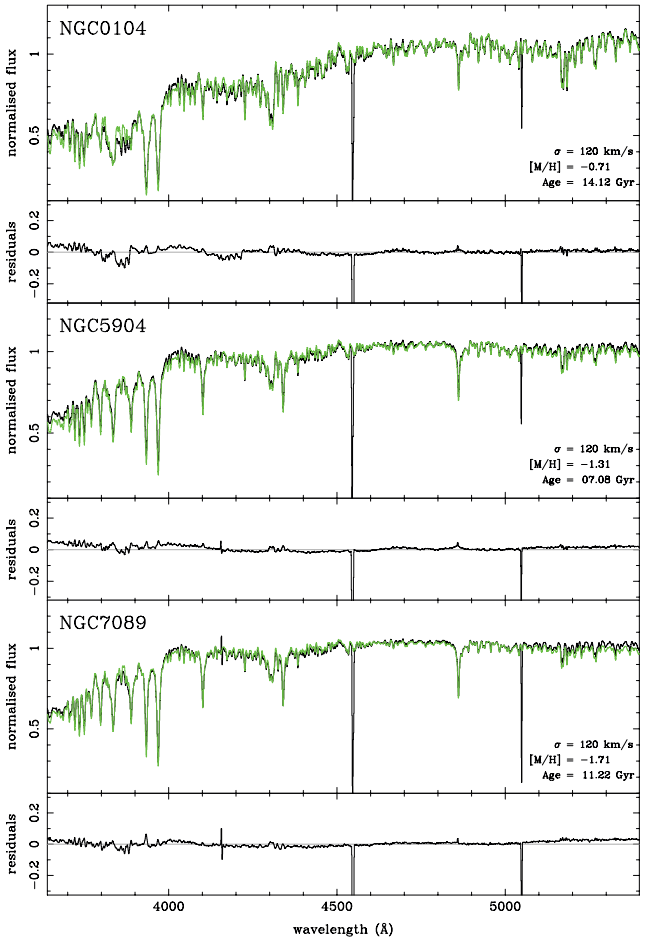

Figure 20. Spectra of various representative Galactic GCs with varying metallicities, from Schiavon et al. (2005), plotted in black. For each cluster, we overplot in green the best-fitting SSP SED. We adopt for the models a Kroupa universal IMF. The age and metallicity of the SSP are indicated within each panel. The SSP SEDs were smoothed to match the instrumental resolution of the observations (i.e. $\sigma = 120\,\mathrm{km\,s^{-1}}$). The residuals obtained are plotted at the same scale. Note that no continuum removal was applied when performing the fit.

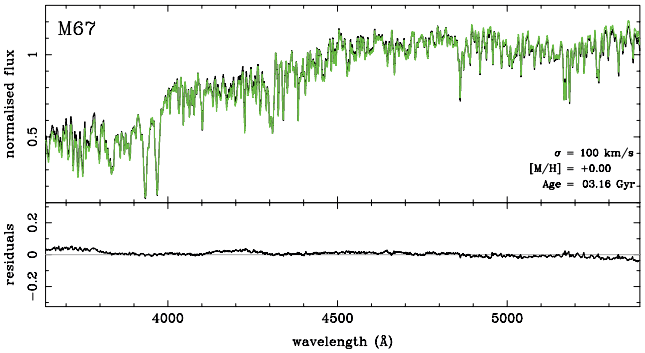

Figure 21. The spectrum of the Milky Way open cluster M67 (Schiavon et al. 2004) plotted in black. We overplot the best-fitting SSP SED in green, with its age and metallicity indicated within the panel. We adopt a Kroupa universal IMF. The model has been smoothed to match the instrumental resolution of the observed spectrum (also quoted). The residuals are plotted in the bottom panel with the same scale. Note that no continuum removal was applied for performing the fit.

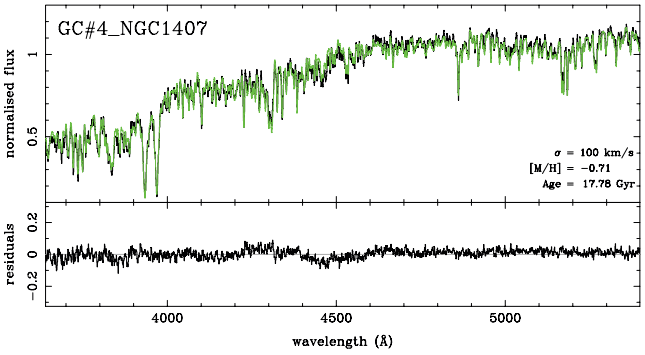

Figure 22. The spectrum of a bright GC of the galaxy NGC 1407, from Cenarro et al. (2007b), plotted in black. We overplot the best-fitting SSP SED in green, with its age and metallicity indicated within the panel. We adopt a Kroupa universal IMF. The model has been smoothed to match the instrumental resolution of the observed spectrum (also quoted). The residuals are plotted in the bottom panel with the same scale. Note that no continuum removal was applied for performing the fit.

propose to use our base models in the same way as we describe in Section 6.2.1 to deal with such abundance patterns.

We illustrate in Fig. 22 the potential use of these models for the study of extragalactic GC systems. We plot a Keck/LRIS spectrum of a GC of the massive elliptical galaxy NGC 1407 (Cenarro et al. 2007b), with a mean S/N of ∼40. The model SEDs were properly smoothed to match the resolution of the observed spectrum ($\sigma \sim 100\,\mathrm{km\,s^{-1}}$). We obtain an age of 17.78 Gyr and a metallicity of [M/H] = −0.71 in agreement, within the errors, with the values derived from the detailed line-strength analysis performed by these authors.

6.1.1 Using line-strength indices to estimate GC ages and metallicities

The line strengths derived from our base models have already been compared to the line strengths of the integrated spectra of Galactic GCs (e.g. Mendel, Proctor & Forbes 2007; Cenarro et al. 2008; Cervantes & Vazdekis 2009). These comparisons confirm the well-known model zero-point problem affecting the age estimates obtained from the Balmer lines, i.e. the derived ages are larger than the CMD-derived ages. Note that the same problem appears when using other models. For an extensive description and discussion of this problem, we refer the reader to the above papers and to e.g. Gibson et al. (1999), Vazdekis et al. (2001a) and Schiavon et al. (2002).

In Fig. 23, we plot several line-strength diagnostic diagrams to obtain the ages and metallicities of the Galactic GC sample of Schiavon et al. (2005). We use, for this purpose, our reference models and the alternative set of models described in Section 2.3.1, which adopt the recently published temperature scale of González-Hernández & Bonifacio (2009). We see that the data fall outside the model grid towards ages larger than the oldest predicted SSP (see also Fig. 12). This is older than the ages derived from CMDs. If we use the model grid that adopts the González-Hernández & Bonifacio (2009) temperature scale we obtain, however, lower $H\beta_o$ values, i.e. we alleviate in part the model zero-point problem obtaining slightly younger ages for the GCs than with the reference models, using the MILES temperatures. This is because when synthesizing an SSP SED the code assigns a cooler spectrum (i.e. with lower Balmer index values) to a requested star of given parameters, as the González-Hernández & Bonifacio (2009) temperatures are ∼51 K

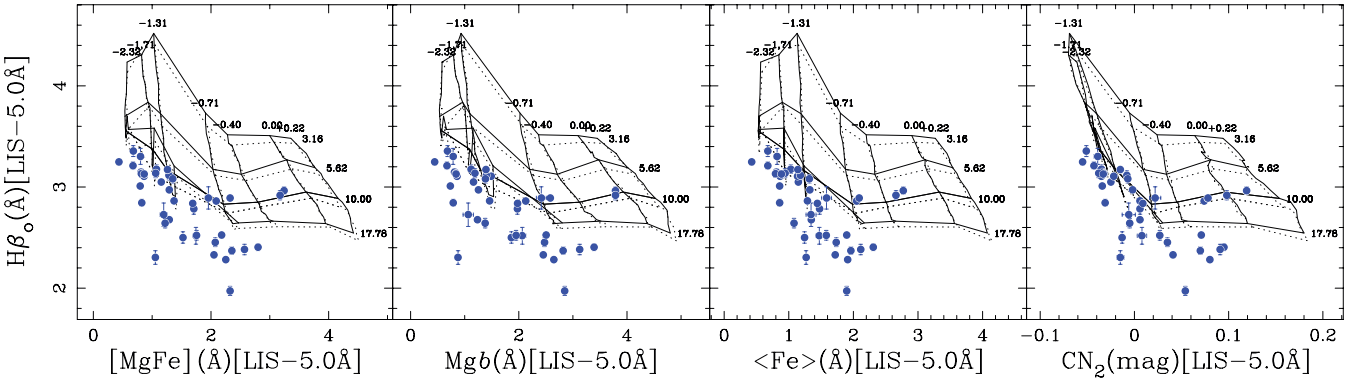

Figure 23. The Hβ_o age indicator of Cervantes & Vazdekis (2009) is plotted versus various metallicity indices, all measured at the LIS-5.0 Å resolution, for the Galactic GC sample of Schiavon et al. (2005). Overplotted are our reference models (solid lines), which adopt the MILES temperatures, and another set of models that adopt the recently published temperature scale of González-Hernández & Bonifacio (2009) (dotted lines). SSP metallicities are quoted on the top of the model grid, just above the line corresponding to the youngest stellar populations (i.e. 3.16 Gyr). We indicate the age of the SSPs (in Gyr) for the most metal-rich models (i.e. [M/H] = +0.22).

hotter than in MILES. Also note that these models provide slightly larger values for the metallicity indices. However, as pointed out in Section 2.3.1, we do not find a strong physical reason to use the González-Hernández & Bonifacio (2009) temperature scale, particularly for metal-rich objects. Note that Fig. 23 also shows that a significantly larger temperature offset (∼150 K), i.e. much larger than the current uncertainties in the temperature scale, is required to be able to overcome the model zero-point. Therefore other aspects, such as those discussed in Vazdekis et al. (2001a) and Schiavon et al. (2002), should be considered.

The large age sensitivity of the Hβ_o index is remarkable, which allows us to obtain nearly orthogonal model grids, particularly for [M/H] > −0.71. We see that our age estimates for the most metal-rich GCs do not depend on the metallicity indicator in use. However, the metallicities obtained might differ among the plotted diagnostic diagrams, indicating a departure from the scaled-solar abundance pattern. In fact, based on the Hβ_o versus CN_2 diagram we obtain for many GCs metallicities that are significantly larger than the ones inferred from the Hβ_o versus [MgFe] plot. Therefore these clusters show CN_2 values that are larger than expected according to their total metallicities, as traced by the [MgFe] index (e.g. Thomas et al. 2003). Note that a characteristic CN-strong pattern emerged in the residuals obtained from the full spectrum fits shown in Fig. 20.

Finally, note that these index–index diagrams show that there are a group of clusters with apparently younger ages. Cenarro et al. (2008) found a clear correspondence between the Hβ values and the specific frequency of blue stragglers (BSS), such that the higher the BSS ratio the younger the apparent spectroscopic age. We refer the reader to that paper for further details.

6.2 Galaxies

In this section, we show the use of our models for studying galaxy spectra. With this aim we have chosen four galaxies (out of 14) of the Virgo early-type galaxy sample of Yamada et al. (2006), with spectra of an extraordinarily high S/N (S/N > 100 Å^{-1} at the Hγ feature), extracted within an aperture of r_e/10. Our subsample of galaxies (NGC 4387, 4473, 4489 and 4621) covers a range in age, metallicity, abundance ratio and mass, as these galaxies were selected alongside the colour–magnitude relation of the Virgo cluster. The resolution of the Subaru spectrum for NGC 4489 is FWHM = 3.1 Å, whereas for the other three galaxies, observed at the WHT (Vazdekis et al. 2001b), the resolution is FWHM = 2.4 Å. Such high quality spectra were obtained to be able to measure the Hγ_σ age indicator of Vazdekis & Arimoto (1999), which is virtually insensitive to metallicity. Mean luminosity weighted ages and metallicities were obtained by plotting Hγ_σ versus the total metallicity indicator [MgFe] (González 1993; Vazdekis et al. 2001b; Thomas et al. 2003). The derived values are tabulated in table 5 of Yamada et al. (2006). We did not attempt here to fit the spectra of these galaxies, but in Fig. 24 we overplot for each galaxy the SSP SED with the closest age and metallicity, as listed in their table 5. The model SEDs were smoothed to match the total resolution of the galaxy spectra (i.e. taking into account the instrumental resolution and galaxy velocity dispersion), which are indicated in the panels.

The residuals of the comparison for the low-velocity dispersion (σ), old galaxy, NGC 4387, are very small. For the other galaxy with low σ but young age, NGC 4489, the residuals in the blue part are as small as those obtained for NGC 4387. However, we see a pattern in the residuals at longer wavelengths. If the stars of this galaxy would have formed in two bursts then a characteristic residual pattern would be seen, namely a surplus of light in the blue and a deficit in the red, which is not the case. The good flux calibration of the models presented here allows this type of analysis. Unlike the other galaxies, the spectrum of NGC 4489 was taken in one of the Subaru observing runs, for which the correction of the continuum shape to a flux scale is less accurate than is achieved for the observing runs at the WHT. The same applies to the feature seen in the residuals at ∼4225 Å.

6.2.1 Dealing with abundance ratios using the base models

For the most massive galaxies, NGC 4473 and NGC 4621, we see in Fig. 24 positive residuals for the Fe features, e.g. Fe4383, Fe5270, Fe5335, and negative residuals for the Mg feature at ∼5170 Å. This shows the well-known [Mg/Fe] enhancement, which is characteristic of massive galaxies (e.g. Peletier 1989; Worthey, Faber & González 1992; González 1993).

We show here how our base models can be safely used for studying galaxies with non-solar element mixtures. A good example of such use is shown in the line-strength analysis of Yamada et al. (2006). A proxy for the [Mg/Fe] abundance ratio is obtained

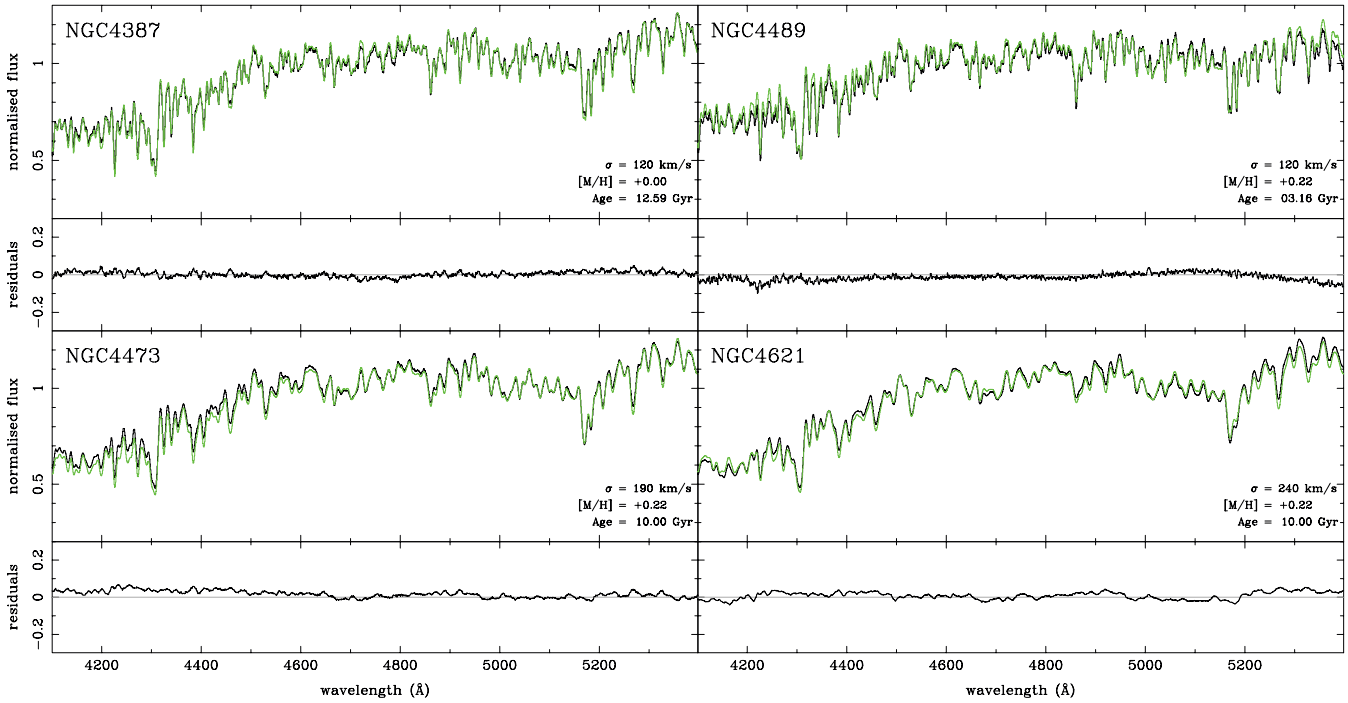

Figure 24. Various Virgo elliptical galaxies from the sample of Yamada et al. (2006), with S/N > 100 Å^{-1} at the Hγ feature, are plotted in black. For each galaxy we overplot in green the SSP SED, with the Kroupa universal IMF, corresponding to the age and metallicity (indicated within each panel), which have been derived by these authors via the Hγ_σ versus [MgFe] diagnostic diagram. The model spectra were smoothed to match the total resolution of the spectra (also indicated within the panels). Note that no continuum correction was applied. The residuals are plotted within the panels with the same scale.

with the aid of the base model grids and an age indicator that is almost insensitive to metallicity. If a galaxy spectrum is enhanced in Mg/Fe, we obtain a higher metallicity when this age indicator is plotted versus an Mg-dominated index than when the index is Fe-dominated. Yamada et al. use the Hγ_σ index of Vazdekis & Arimoto (1999), which requires spectra with an extremely high S/N and the metallicity indicators Mg*b* and Fe3 ($\equiv \frac{\mathrm{Fe4383+Fe5270+Fe5335}}{3}$ defined in Kuntschner 2000). Irrespective of the metallicity indicator in use, such optimized age indicators provide orthogonal model grids, and the lines of constant age are essentially horizontal, which means that a given measurement for the age indicator corresponds to a unique age (see Cervantes & Vazdekis 2009). The metallicity difference obtained in this way, [$Z_{\mathrm{Mg}}/Z_{\mathrm{Fe}}$], is a good proxy for the abundance ratio [Mg/Fe], as was shown in e.g. Sánchez-Blázquez et al. (2006c), de la Rosa et al. (2007) and Michielsen et al. (2008). In Fig. 25 we plot the values obtained by Yamada et al. (2006, table 5) for this proxy versus the [Mg/Fe] estimates derived with the aid of the models of Thomas et al. (2003), which specifically account for non-scaled-solar element partitions. To apply these models, we use the Lick/IDS version of the Hβ, Mg*b* and Fe3 indices of Yamada et al. (2006). As an example, table 5 of Yamada et al. lists [$Z_{\mathrm{Mg}}/Z_{\mathrm{Fe}}$] $\sim$ 0.6 for NGC 4473 and 4621. Following Fig. 25, this translates to [Mg/Fe] $\sim$+0.25 on the abundance ratio scale of Thomas et al. (2003). Note that this [Mg/Fe] abundance scale is also a considerable approximation because (i) of the use of scaled-solar isochrones, (ii) it is based on three synthetic spectra to model the SSPs and (iii) a fixed element ratio pattern is adopted. Also note that in Fig. 25, we combine the results from two different model predictions and that our method requires extrapolating to higher metallicities to obtain Z_{Mg} (see the corresponding plots in Yamada et al. 2006). This explains in part the larger dispersion obtained for the higher abundance ratios.

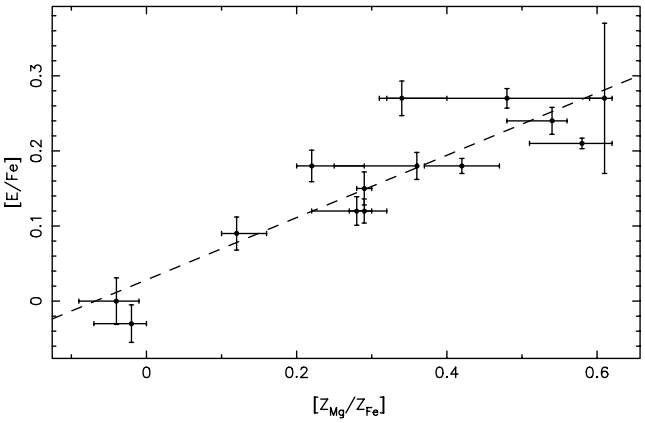

Figure 25. [$Z_{\mathrm{Mg}}/Z_{\mathrm{Fe}}$] versus [Mg/Fe] abundance ratio estimates for the Virgo elliptical galaxies of Yamada et al. (2006). The proxy for the abundance ratio is the metallicity difference derived from plotting the Hγ_σ age indicator of Vazdekis & Arimoto (1999) versus the magnesium-dominated index, Mg*b*, and Hγ_σ versus the iron-dominated index, Fe3. We plot the [$Z_{\mathrm{Mg}}/Z_{\mathrm{Fe}}$] values listed in table 5 of Yamada et al. To estimate the [Mg/Fe] abundance ratio, we use the Lick/IDS indices and the models of Thomas et al. (2003).

It is worth noting that the newly defined Hβ_o index of Cervantes & Vazdekis (2009) provides similar age disentangling power as the Hγ_σ index, but with the advantage that Hβ_o requires spectra of similar qualities as usually employed for measuring the standard Hβ index (see Cervantes & Vazdekis 2009). Hβ can also be used for this purpose, but the resulting model grids are significantly less orthogonal, increasing the error bars of the [$Z_{\mathrm{Mg}}/Z_{\mathrm{Fe}}$] determinations.

Finally, to obtain the total metallicity, these optimized age indicators can be plotted versus the combined indices [MgFe] (González 1993) or [MgFe]′ (Thomas et al. 2003), which have been shown to be virtually insensitive to the [Mg/Fe] abundance ratio.

In the second paper of this series we will present an updated version of Fig. 25, where we use both the scaled-solar and the α-enhanced version of our MILES models, in order to be fully consistent. In addition, these models reach higher metallicities, avoiding in this way the extrapolation that might be required to obtain $[Z_{\rm Mg}/Z_{\rm Fe}]$. However, we have shown here that our base models, which combine scaled-solar isochrones with an empirical stellar library, can be used for studying galaxies with α-enhanced element partitions via the line-strength analyses.

6.2.2 *Cautionary remark on the Hβ model predictions*

Fig. 26 shows the very popular diagnostic diagram Hβ versus [MgFe], which is obtained from our MILES SSP SEDs once smoothed to match the LIS-14.0 Å resolution. For comparison we show the equivalent model grid from the V99 models, as updated in this work, which uses the Jones (1999) stellar spectral library. Fig. 26 shows that the V99 model grid is significantly more orthogonal than the grid obtained with the MILES SSP SEDs, mainly due to the lower sensitivity of the Hβ index to metallicity variations. The MILES SSP grid looks, in fact, more similar to the equivalent standard grid obtained on the basis of the empirical fitting functions of Worthey et al. (1994) on the Lick/IDS system.

We plot the radial line-strength profile for the Virgo galaxy NGC 4387, which has been obtained from low-resolution Keck/LRIS spectra by Sánchez-Blázquez et al. (2007). We deliberately do not plot the observational errors, as we are only interested in illustrating the net effect on the trend. Note that we also plotted in Fig. 24 the higher resolution spectrum obtained at the WHT for the central aperture of $r_e/10$, i.e. 1.6 arcsec (Yamada et al. 2006). According to the V99 model grid, the observed gradient can be attributed to a decreasing metallicity with an increasing galactocentric distance. Using the MILES SSP grid, the gradient can be explained by a combination of increasing age and decreasing metallicity.

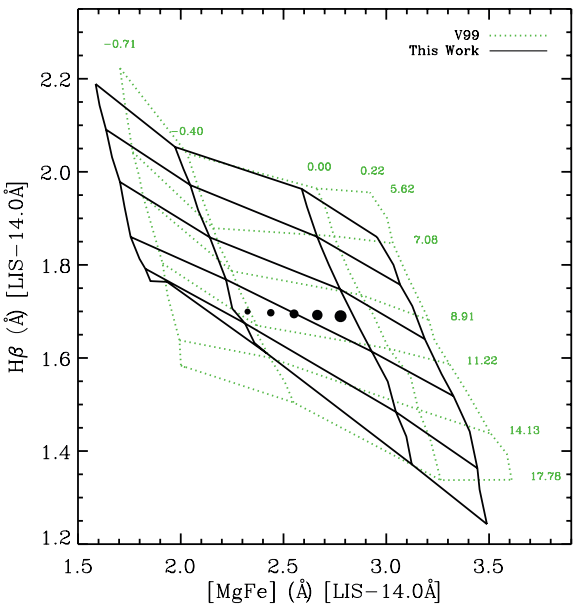

Figure 26. Hβ versus [MgFe] diagnostic diagram obtained from our MILES base model SEDs (solid line) and V99 (dotted line), which uses the Jones (1999) stellar library. The indices were measured on the SSP spectra once smoothed to match the LIS-14.0 Å resolution. We plot the radial line-strength profile for the Virgo galaxy NGC 4387, which has been obtained from low-resolution Keck/LRIS spectra by Sánchez-Blázquez et al. (2007). The size of the filled circles decreases with an increasing galactocentric distance: 1.25, 2.5, 5, 10 and 20 arcsec.

We have investigated the possible cause for the differences between the two model grids. As we use here an updated version for the V99 models, which is now based on the same isochrones and transformations to the observational plane that we employ for the MILES models, these two ingredients cannot be the ones we are looking for. We identified three other possible sources: (i) intrinsic differences in the spectra of MILES and Jones (1999) stellar libraries, mostly around the Hβ feature (such differences have been quoted before by Worthey & Ottaviani 1997); (ii) differences in the stellar parameters adopted here (i.e. C07a) and in V99 and (iii) differences in the algorithms employed for computing/assigning a stellar spectrum to a given set of atmospheric parameters. In order to understand this issue, we synthesized SEDs using the 245 stars, both in the Jones and in the MILES libraries, with the following characteristics: (i) models using both stellar libraries, MILES and Jones; (ii) models using MILES spectra assigning them the two set of stellar parameters, those used in V99 and in MILES; and (iii) models using MILES stellar spectra and with both algorithms, the one used in V99 and the new algorithm described in V03.

For the sake of brevity, we do not show here this detailed study but we summarize the main results. We found that these model differences are mostly originated by the stellar spectrum assignation scheme employed in V99, which works at a significantly more coarse stellar parameter resolution. The other aspects described above also have a significant impact, but to a lesser degree. Furthermore, the Hβ index measurements on the SSP SEDs synthesized with the same algorithm but exchanging the stellar spectral libraries are consistent with the Hβ index measurements obtained on a star-by-star basis. Unfortunately, this problem might have some impact on certain studies that make use of the Hβ index derived from V99 models.

Given the improvement on the stellar spectrum assignation scheme used for the MILES SSPs, we will provide an updated version of the V99 predictions in our website using the new algorithms.

7 THE WEB TOOL

The exploitation of stellar population synthesis models is depended in part on the development of tools by users. Some authors offer software to either help to interpret or aid the user to handle the provided predictions. A few examples include LECTOR (V99), GALAXEV (Bruzual & Charlot 2003), PÉGASE (Fioc & Rocca-Volmerange 1997, 1999) or EZ AGES (Graves & Schiavon 2008). In an effort to continue and extend these initiatives, we have created a new website (http://miles.iac.es) to provide support for using the spectra of both the MILES stellar library and the model predictions described in this paper, but also in V99 at 1.8 Å resolution. The web page also handles the near-IR stellar spectral library CaT and models that we published in Cenarro et al. (2001a,b, 2002) and V03. Line-strength predictions based on empirical fitting functions (including those of the Lick/IDS system) are also included. Furthermore the web page includes photometric quantities such as fluxes, colours, mass-to-light ratios and surface brightness fluctuations, which have been published in Vazdekis et al. (1996) and Blakeslee, Vazdekis & Ajhar (2001). It is very important to note that all these predictions will

be continuously updated with the latest developments and with the feedback from users. These comply with the standards of the Virtual Observatory.

This web page is intended for users not only to retrieve both the stellar spectra and the synthetic SSP SED predictions in this project, but also to provide webtools to facilitate the handling and transformation of the spectra. Beyond the basic tools for the exploration and visualization of the whole data set, at a first stage, we also provide advanced webtools to do the following.

(i) Generate synthetic stellar spectra for a given set of stellar atmospheric parameters. These spectra are computed on the basis of our stellar libraries according to the mathematical algorithm described in appendix B of V03 (see also Section 2.3).

(ii) Transform the stellar spectra or the SSP spectra to the instrumental set-up of the data observed by the user. This tool will allow the user to input the details of the instrumental configuration of the observed data (spectral resolution and sampling) and generate a set of spectra matching that set-up. The model/library spectra will be convolved with the observational point spread function (PSF; typically Gaussian) to match the spectral resolution of the observed data. During this step, particular attention will be paid as to whether the user requires the FWHM to be constant as a function of wavelength (in which case convolution will be performed in linear space) or constant in velocity (in which case convolution will be performed in logarithmic space). Finally, the data will be rebinned (i.e. spectrally sampled and, if desired, in log scale).

(iii) Measure a variety of line-strength indices and colours on the spectra. We make use of LECTOR (V99) and INDEXF (Cardiel 2007) for this purpose. This tool allows us to input newly defined indices by the user.

(iv) Convert Lick/IDS line-strength indices to the new LIS proposed here. We use for this purpose the transformations described in Appendix A.

(v) Estimate the best luminosity weighted age and metallicity and α-enhancement for a given set of line indices using RMODEL (Cardiel et al. 2003). This program determines stellar population parameters (e.g. age, metallicity, IMF type and slope), using as input line-strength indices by interpolating SSP model predictions. Both linear and bivariate fits are computed to perform the interpolation.

(vi) Provide spectra for a given star formation history.

These tools are intended to be the first of many more sophisticated tools that we will incorporate in the website over time, to facilitate the comparison between the observed data and our stellar library and models, and in this way make the analysis easier.

8 SUMMARY AND CONCLUSIONS

Here we present stellar population model SEDs based on the empirical stellar spectral library MILES. In SB06a we have presented and described this library, whereas in C07a we have published the stellar parameter determinations. Here we present synthetic SEDs for single-age, SSPs covering the full optical spectral range, 3540.5–7409.6 Å, at moderately high resolution, FWHM = 2.3 Å, which is virtually constant as a function of wavelength (see fig. 4 of SB06a). The SSP SEDs have a reliable, accurate flux calibration, which is one of the major advantages of the MILES library. Furthermore, the redder part of the SSP spectra does not show telluric residuals, as these were carefully cleaned from the stellar spectra as shown in SB06a.

We consider the SEDs presented here as our base models, as they combine an empirical library, which is imprinted with the chemical composition of the solar neighbourhood, with scaled-solar stellar isochrones (Girardi et al. 2000). Therefore, whereas our models are self-consistent, and scaled-solar for solar metallicity, this is not the case for the low metallicity regime, as the observed stars there do not show this abundance pattern (see Schiavon 2007). In a second paper we will present self-consistent models, both scaled-solar and α-enhanced, for a range in metallicities. For this purpose we have used MILES, together with theoretical model atmospheres, which are coupled to the appropriate stellar isochrones.

An interesting feature of our base models is that they rely, as much as possible, on empirical ingredients. Apart from using MILES stellar spectra, we also use transformations of the theoretical parameters of the isochrones to observational, measurable, quantities that are based on extensive empirical, photometric libraries, with marginal dependence on model atmospheres. The implementation of MILES in the population synthesis code has been done very carefully: each star of the library has been compared with other MILES stars with similar atmospheric parameters, using the same interpolation algorithm used in the synthesis code. As a result of these tests and other considerations, we have removed or decreased the weight with which a given star contributes to the synthesis of a stellar spectrum for 135 (out of 985) stars of MILES.

The unprecedented stellar parameter coverage of the MILES library has allowed us to safely extend our optical SSP SEDs from intermediate to very old age regimes (0.06–18 Gyr) and the metallicity coverage of the SSPs from super-solar ([M/H] = +0.22) to [M/H] = −2.32. The very low metallicity SSPs should be of particular interest for GC studies. In addition, we have computed SSP SEDs for a suite of IMF shapes and slopes: unimodal and bimodal IMF shapes as defined in Vazdekis et al. (1996) with slopes varying in the range of 0.3–3.3 (Salpeter: unimodal with slope 1.3), and the segmented IMFs of Kroupa (2001) (universal and revised cases). In addition to our reference models, which adopt the MILES temperatures published in C07a, we provide an alternative set of models that adopt the recently published temperature scale of González-Hernández & Bonifacio (2009) (i.e. about ∼51 K hotter). The most relevant feature of these models is that the well-known model zero-point problem affecting the age estimates obtained from the Balmer lines, i.e. the ages obtained are larger than the CMD-derived ages, is partially alleviated.

To constrain the range of ages, metallicities and IMFs where the use of these SEDs is safe, we provide a quantitative analysis. This analysis, which basically takes into account the parameter coverage of the stellar library feeding the models, clearly shows that our SSP SEDs can be safely used in the age range of 0.06–18 Gyr, and for all the metallicities, except for [M/H] = −2.32, for which only stellar populations with ages above ∼10 Gyr can be considered safe. This applies to the standard IMF shapes. However our quantitative analysis has shown that the quality of the SSP SEDs decreases as we increase the IMF slope, especially for the unimodal IMF. For example, for slopes above 1.8, the synthesized SSP SEDs for [M/H] = −2.32 are no longer safe for a unimodal IMF. According to this analysis, our predictions are of significantly higher quality than any previous model predictions in the literature for all the ages and metallicities that have been computed in this work. For example, any predictions based on the standard fitting functions of the Lick/IDS system (Worthey et al. 1994), e.g. line-strength indices, with which most stellar population studies have been performed so far, should not be considered safe for [M/H] < −1.3 (for standard IMF shapes). This limit is set at higher metallicity, [M/H] ∼ −0.7, for predictions based on STELIB (e.g. Bruzual & Charlot 2003). The comparison of our new models, based on MILES, with the SSP

SEDs published in V99 reveals systematic differences due to limitations in the flux calibration of the Jones (1999) stellar library that feeds the latter models. As for the line strengths the most important difference between these two models is found for the Hβ index, which shows a lower metallicity sensitivity in the V99 models. We show an example where this effect has a non-negligible impact on our interpretation of galaxy age/metallicity gradients.

The SSP SEDs increase our ability to perform the analysis of stellar populations, which can be done in a very flexible manner. Observed spectra can be studied by fitting the full spectrum or by focusing on selected line indices, either standard or newly defined. An example of the previous method can be found in Koleva et al. (2008), where various stellar population models were compared following this approach. Our favourite approach is to analyse the spectrum of a galaxy at the resolution imposed by its velocity dispersion (and its instrumental resolution), which requires us to smooth the SSP SEDs to match the observed total resolution. Therefore, the line index analysis to obtain relevant stellar population parameters is performed in the system of the galaxy, through either full spectrum fitting or line index approaches.

As many authors prefer to plot the line-strength measurements of their whole galaxy sample in a single index–index diagnostic diagram, or to compare their data to tabulated indices in the literature, we propose a new LIS, which makes this method straightforward to apply. With LIS we avoid the well-known uncertainties inherent to the widely employed Lick/IDS system. Unlike the latter, LIS has two main advantages, i.e. a constant resolution as a function of wavelength and a universal flux-calibrated spectral response. Data can be analysed in this system at three different resolutions: 5, 8.4 and 14 Å (FWHM), i.e. $\sigma = 127$, 214 and 357 km s^{-1} at 5000 Å, respectively. These resolutions are appropriate for studying GC, low- and intermediate-mass galaxies, and massive galaxies, respectively. Line-strength measurements given at a higher LIS resolution can be smoothed to match a lower LIS resolution. Furthermore, we provide polynomials to transform current Lick/IDS line index measurements in the literature to the new system. We provide LIS line index tables for various popular samples of Galactic GCs and galaxies. We also show various popular index–index diagnostic diagrams for these samples in the LIS system.

As an application, we have fitted a number of representative stellar clusters of varying ages and metallicities with our models, obtaining good agreement with CMD determinations. Unlike for the open cluster M67, our SED fits for a sample of Galactic GCs show non-negligible residuals bluewards of 4300 Å, which mostly reflect the characteristic CN-strong features of these clusters among other deviations from the scaled-solar pattern. We also applied our models to representative galaxies with high quality spectra, for which independent studies are available, obtaining good results. We show that our base models can be used for studying line-strength indices of galaxies with α-enhanced element partitions. Examples of such a use can be found in e.g. Vazdekis et al. (2001b), Kuntschner et al. (2002), Carretero et al. (2004) and Yamada et al. (2006). The method consists in plotting a highly sensitive age indicator, such as that of Vazdekis & Arimoto (1999), or the recently defined Hβ_o index of Cervantes & Vazdekis (2009) versus Mg (e.g. Mg*b*) and versus Fe (e.g. Fe4383, $\langle$Fe$\rangle$), obtaining a virtually orthogonal model grid where the estimated age does not depend on the metallicity indicator in use. Unlike the age, for an [Mg/Fe] enhanced galaxy, the metallicities obtained differ when plotted against, for example, Mg*b* and $\langle$Fe$\rangle$ indices. This metallicity difference, $[Z_{\mathrm{Mg}b}/Z_{\langle\mathrm{Fe}\rangle}]$, can be used as a good proxy for the abundance ratio determined with the aid of stellar population models that specifically take into account non-solar element partitions. Although this proxy yields larger [Mg/Fe] values, there is a linear relation between these two ways of estimating the abundance ratios (e.g. Sánchez-Blázquez et al. 2006c; de la Rosa et al. 2007; Michielsen et al. 2008). In the second paper of this series we will present both α-enhanced and scaled-solar self-consistent SSP SEDs, all based on MILES, but modified with the aid of model atmospheres. By applying these models to galaxies with varying abundance ratios, for which high S/N spectra are available, we confirm the linear relation mentioned above. There is one advantage in using this proxy: the abundance ratios determined in this way do not depend on the specific details of modelling of α-enhanced stellar populations such as those that are implicit to the computations of the atmosphere, or the adopted element mixtures.

Our fits to the stellar cluster and galaxy spectra of high quality have confirmed the high precision of the flux calibration of our SSP SEDs. Furthermore, the colours that we obtained from our SSP SEDs are consistent with the ones that we derived via the employed photometric stellar libraries, within typical zero-point uncertainties. Such agreement shows the reliability of the temperatures adopted for the MILES stars (C07a), which are consistent with the temperature scales of Alonso et al. (1996, 1999). Such accuracy opens new applications for these models. For example, the model SEDs can be used as templates for codes aiming at determining spectrophotometric redshifts, particularly for those based on narrow-band filters (e.g. ALHAMBRA, PAU).

Finally we present a web page from which not only these models and stellar libraries can be downloaded, but where we also provide a suite of user-friendly webtools to facilitate the handling and transformation of the spectra. For example, once the user enters the details of the instrumental set-up employed in the observations (e.g. PSF, sampling), the users can obtain their favourite line-strength indices and diagnostic diagrams, ready to plot their observational measurements. Apart from the model SEDs shown here, the web page also provides predictions for a suite of observable quantities.

ACKNOWLEDGMENTS

We are indebted to the Padova group for making available their isochrone calculations. We are grateful to P. Coelho, J. L. Cervantes, I. G. de la Rosa, M. Koleva, E. Ricciardelli and J. González-Hernández for very useful discussions. We would also like to thank J. A. Perez Prieto for helping us in the construction of the web page for the models. We thank the referee for pointing out relevant aspects that were useful for improving the original manuscript. The MILES library was observed at the INT on the island of La Palma, operated by the Isaac Newton Group at the Observatorio del Roque de los Muchachos of the Instituto de Astrofísica de Canarias. This research has made an extensive use of the SIMBAD data base (operated at CDS, Strasbourg, France), the NASA's Astrophysics Data System Article Service and the *Hipparcos* Input Catalogue. PSB acknowledges the support of a Marie Curie Intra-European Fellowship within the 6th European Community Framework Programme. JFB acknowledges support from the Ramón y Cajal Program financed by the Spanish Ministry of Science and Innovation. AJC is a *Ramón y Cajal* Fellow of the Spanish Ministry of Science and Innovation. This work has been supported by the Programa Nacional de Astronomía y Astrofísica of the Spanish Ministry of Science and Innovation under grants AYA2007-67752-C03-01, AYA2007-67752-C03-02 and AYA2006-15698-C02-02.

REFERENCES

Alexander D. R., Ferguson J. W., 1994, ApJ, 437, 879
Alonso A., Arribas S., Martínez-Roger C., 1995, A&A, 297, 197
Alonso A., Arribas S., Martínez-Roger C., 1996, A&A, 313, 873
Alonso A., Arribas S., Martínez-Roger C., 1999, A&AS, 140, 261
Beasley M. A., Strader J., Brodie J., Cenarro J., Geha M., 2006, AJ, 131, 814
Beasley M. A., Cenarro J., Strader J., Brodie J., 2009, AJ, 137, 5146
Bernardi M. et al., 2003a, AJ, 125, 1817
Bernardi M. et al., 2003b, AJ, 125, 1849
Bernardi M. et al., 2003c, AJ, 125, 1866
Bertelli G., Bressan A., Chiosi C., Fagotto F., Nasi E., 1994, A&AS, 106, 275
Bessell M. S., Brett J. M., Wood P. R., Scholz M., 1989, A&AS, 77, 1
Bessell M. S., Brett J. M., Scholz M., Wood P. R., 1991, A&AS, 89, 335
Blakeslee J. P., Vazdekis A., Ajhar E. A., 2001, MNRAS, 320, 193
Blackwell D. E., Petford A. D., Arribas S., Haddock D. J., Selby M. J., 1990, A&A, 232, 396
Bohlin R. C., Gilliland R. L., 2004, AJ, 127, 3508
Bruzual G., Charlot S., 2003, MNRAS, 344, 1000
Bruzual G., 2007, in Vazdekis A., Peletier R., eds, Proc. IAU Symp. 241, Stellar Populations as Building Blocks of Galaxies. Cambridge Univ. Press, Cambridge, p. 125
Burstein D., Faber S. M., Gaskell C. M., Krumm N., 1984, ApJ, 287, 586
Buser R., Kurucz R. L., 1978, A&A, 70, 555
Buzzoni A., 1995, ApJS, 98, 69
Cappellari M., Emsellem E., 2004, PASP, 116, 138
Cardiel N., 2007, in Figueras F. et al., eds, Proc. 7th Scientific Meeting of the Spanish Astronomical Society, Highlights of Spanish Astrophysics IV. Springer, Berlin, CD-ROM
Cardiel N., Gorgas J., Sánchez-Blázquez P., Cenarro A. J., Pedraz S., Bruzual G., Klement J., 2003, A&A, 409, 511
Carretero C., Vazdekis A., Beckman J., Sánchez-Blázquez P., Gorgas J., 2004, ApJ, 609, L45
Casagrande L., Portinari L., Flynn C., 2006, MNRAS, 373, 13
Cassisi S., Salaris M., Castelli F., Pietrinferni A., 2004, ApJ, 616, 498
Cenarro A. J., Cardiel N., Gorgas J., Peletier R. F., Vazdekis A., Prada F., 2001a, MNRAS, 326, 959
Cenarro A. J., Gorgas J., Cardiel N., Pedraz S., Peletier R. F., Vazdekis A., 2001b, MNRAS, 326, 981
Cenarro A. J., Gorgas J., Cardiel N., Vazdekis A., Peletier R. F., 2002, MNRAS, 329, 863
Cenarro A. J. et al., 2007a, MNRAS, 374, 664 (C07a)
Cenarro A. J., Beasley M. A., Strader J., Brodie J., Forbes D., 2007b, AJ, 134, 391
Cenarro A. J., Cervantes J. L., Beasley M. A., Marin-Franch A., Vazdekis A., 2008, ApJ, 689, L29
Cervantes J. L., Vazdekis A., 2009, MNRAS, 392, 691
Cerviño M., Valls-Gabaud D., Luridiana V., Mas-Hesse J. M., 2002, A&A, 381, 51
Chilingarian I. V., Prugniel P., Sil'Chenko O. K., Koleva M., 2007, in Vazdekis A., Peletier R., eds, Proc. IAU Symp. 241, Stellar populations as Building Blocks of Galaxies. Cambridge Univ. Press, Cambridge, p. 175
Chomiuk L., Strader J., Brodie J., 2008, AJ, 136, 234
Cid Fernandes R., Mateus A., Sodré L., Stasińska G., Gomes J. M., 2005, MNRAS, 358, 363
Cid Fernandes R., González-Delgado R., 2010, MNRAS, in press (arXiv:0912.0410)
Coelho P., Barbuy B., Meléndez J., Schiavon R. P., Castilho B. V., 2005, A&A, 443, 735
Coelho P., Bruzual G., Charlot S., Weiss A., Barbuy B., Ferguson J., 2007, MNRAS, 382, 498
Covino S., Galletti S., Pasinetti L. E., 1995, A&A, 443, 735
Dalle Ore C., Faber S. M., Gonzalez J. J., Stoughton R., Burstein D., 1991, ApJ 375, 427
de la Rosa I. G., de Carvalho R. R., Vazdekis A., Barbuy B., 2007, AJ, 133, 330
de Vaucouleurs G., de Vaucouleurs A., Corwin H. G. Jr, Buta R. J., Paturel G., Fouqué P., 1991, Third Reference Catalogue of Bright Galaxies. Springer, New York
de Zeeuw P. T. et al., 2002, MNRAS, 329, 513
Edvardsson B., Andersen J., Gustafsson B., Lambert D. L., Nissen P. E., Tomkin J., 1993, A&AS, 102, 603
Falcón-Barroso J., Balcells M., Peletier R., Vazdekis A., 2003, A&A, 405, 455
Fioc M., Rocca-Volmerange B., 1997, A&A, 326, 950
Fioc M., Rocca-Volmerange B., 1999, preprint (astro-ph/9912179)
Fluks M. A., Plez B., Thé P. S., de Winter D., Westerlund B. E., Steenman H. C., 1994, A&AS, 105, 311
Gibson B. K., Madgwick D. S., Jones L. A., Da Costa G. S., Norris J. E., 1999, AJ, 118, 1268
Girardi L., Bressan A., Chiosi C., Bertelli G., Nasi E., 1996, A&AS, 117, 113
Girardi L., Bressan A., Bertelli G., Chiosi C., 2000, A&AS, 141, 371
González J. J., 1993, PhD thesis, Univ. Santa Cruz
González-Hernández J., Bonifacio P., 2009, A&A, 497, 497
González-Delgado R., Cerviño M., Martins L. P., Leitherer C., Hauschildt P. H., 2005, MNRAS, 357, 945
Gorgas J., Faber S. M., Burstein D., González J. J., Courteau S., Prosser C., 1993, ApJS, 86, 153
Gorgas J., Cardiel N., Pedraz S., González J. J., 1999, A&AS, 139, 29
Graves G. J., Schiavon R. P., 2008, ApJS, 177, 446
Harris W., 1996, AJ, 112, 1487
Hayes D. S., 1985, in Hayes D. S., Pasinetti L. E., Philip A. G. D., eds, Proc. IAU Symp. 111, Calibration of Fundamental Stellar Quantities. Dordrecht, Reidel, p. 225
Jones L. A., 1999, PhD thesis, Univ. North Carolina
Jørgensen I., 1999, MNRAS, 306, 607
Kauffmann G. et al., 2003, MNRAS, 341, 33
Kelson D., Illingworth G., Franx M., van Dokkum P. G., 2006, ApJ, 653, 159
Kholopov P. N. et al., 1998, The Combined General Catalogue of Variable Stars, 4th edn. Sternberg Astronomical Institute, Moscow, http://vizier.u-strasbg.fr/II/214A
Koleva M., Prugniel P., Ocvirk P., Le Borgne D., Soubiran C., 2008, MNRAS, 385, 1998
Korn A. J., Maraston C., Thomas D., 2005, A&A, 438, 685
Kroupa P., 2001, MNRAS, 322, 231
Kuntschner H., 2000, MNRAS, 315, 184
Kuntschner H., Smith R. J., Colless H., Davies R. L., Kaldare R., Vazdekis A., 2002, MNRAS, 337, 172
Kuntschner H., Smith R. J., Colless M., Davies R. L., Kaldare R., Vazdekis A., 2006, MNRAS, 369, 497
Le Borgne J.-F. et al., 2003, A&A, 402, 433
Le Borgne J.-F., Rocca-Volmerange B., Prugniel P., Lancon A., Fioc M., Soubiran C., 2004, A&A, 425, 881
Lee H.-C., Worthey G., 2005, ApJS, 160, 176
Lejeune T., Cuisinier F., Buser R., 1997, A&AS, 125, 229
Lejeune T., Cuisinier F., Buser R., 1998, A&AS, 130, 65
MacArthur L. A., 2005, ApJ, 623, 795
Maraston C., 2005, MNRAS, 362, 799
Maraston C., Thomas D., 2000, ApJ, 541, 126
Marigo P., Girardi L., Bressan A., Groenewegen M. A. T., Silva L., Granato G. L., 2008, A&A, 482, 883
Marin-Franch A. et al., 2009, ApJ, 694, 1498
Mármol-Queraltó E., Cardiel N., Cenarro A. J., Vazdekis A., Gorgas J., Pedraz S., Peletier R. F., Sánchez-Blázquez P., 2008, A&A, 489, 885
Martín-Hernández J. M. et al., 2007, in Vazdekis A., Peletier R., eds, Proc. IAU Symp. 241, Stellar Populations as Building Blocks of Galaxies. Cambridge Univ. Press, Cambridge, p. 99
Martins L. P., Coelho P., 2007, MNRAS, 381, 1329
Mendel J. T., Proctor R. N., Forbes D. A., 2007, MNRAS, 379, 1618
Mermilliod J.-C., Mermilliod M., Hauck B., 1997, A&AS, 124, 349

Meylan G., 2003, in Piotto G., Meylan G., Djorgovski S. G., Riello M. eds, ASP Conf. Ser. Vol. 296, New Horizons in Globular Cluster Astronomy. Astron. Soc. Pac., San Francisco, p. 17
Michielsen D. et al., 2008, MNRAS, 385, 1374
Munari U., Sordo R., Castelli F., Zwitter T., 2005, A&A, 442, 1127
Murphy T., Meiksin A., 2004, MNRAS, 351, 1430
Norris J., Freeman K. C., 1979, ApJ, 230, L19
Norris M. A. et al., 2008, MNRAS, 385, 40
Ocvirk P., Pichon C., Lancon A., Thiébaut E., 2006a, MNRAS, 365, 46
Ocvirk P., Pichon C., Lancon A., Thiébaut E., 2006b, MNRAS, 365, 74
Panter B., Heavens A. F., Jimenez R., 2003, MNRAS, 343, 1145
Peletier R. J., 1989, PhD thesis, Univ. Groningen
Percival S. M., Salaris M., 2009, ApJ, 703, 1123
Pierce M. et al., 2006a, MNRAS, 366, 1253
Pierce M. et al., 2006b, MNRAS, 368, 325
Pietrinferni A., Cassisi S., Salaris M., Castelli F., 2004, ApJ, 612, 168
Proctor R., Forbes D., Beasley M. A., 2004, MNRAS, 355, 1327
Prugniel Ph., Soubiran C., 2001, A&A, 369, 1048
Prugniel Ph., Soubiran C., 2004, preprint (astro-ph/0409214)
Prugniel P., Soubiran C., Koleva M., Le Borgne D., 2007, preprint (astro-ph/0703658)
Puzia T. H., Saglia R. P., Kissler-Patig M., Maraston C., Greggio L., Renzini A., Ortolani S., 2002, A&A, 395, 45
Puzia T. et al., 2004, A&A, 415, 123
Ramírez I., Meléndez J., 2005, ApJ, 626, 446
Rodríguez-Merino L. H., Chavez M., Bertone E., Buzzoni A., 2005, ApJ, 626, 411
Rose J. A., 1985, AJ, 90, 1927
Rose J. A., 1994, AJ, 107, 206
Rose J. A., Tripicco M. J., 1986, AJ, 92, 610
Salaris M., Groenewegen M., Weiss A., 2000, A&A, 355, 299
Salpeter E. E., 1955, ApJ, 121, 161
Sánchez-Blázquez P., Gorgas J., Cardiel N., Cenarro J., González J. J., 2003, ApJ, 590, L91
Sánchez-Blázquez P. et al., 2006a, MNRAS, 371, 703 (SB06a)
Sánchez-Blázquez P., Gorgas J., Cardiel N., González J. J., 2006b, A&A, 457, 787
Sánchez-Blázquez P., Gorgas J., Cardiel N., González J. J., 2006c, A&A, 457, 809
Sánchez-Blázquez P., Gorgas J., Cardiel N., 2006d, A&A, 457, 823
Sánchez-Blázquez P., Forbes D. A., Strader J., Brodie J., Proctor R., 2007, MNRAS, 377, 759
Sánchez-Blázquez P. et al., 2009, A&A, 499, 47
Sarzi M. et al., 2006, MNRAS, 366, 1151
Schiavon R. P., 2007, ApJS, 171, 146
Schiavon R. P., Barbuy B., Bruzual G., 2000, ApJ, 532, 453
Schiavon R. P., Faber S. M., Castilho B. V., Rose J. A., 2002, ApJ, 580, 850
Schiavon R. P., Caldwell N., Rose J. A., 2004, AJ, 127, 1513
Schiavon R. P., Rose J. A., Courteau S., MacArthur L., 2005, ApJS, 160, 163
Soubiran C., Katz D., Cayrel R., 1998, A&AS, 133, 221
Strader J., Brodie J., Cenarro A. J., Beasley M. A., Forbes D. A., 2005, AJ, 130, 1315
Tantalo R., Chiosi C., Bressan A., 1998, A&A, 333, 419
Tantalo R., Chiosi C., Piovan L., 2007, A&A, 462, 481
Thomas D., Maraston C., Bender R., 2003, MNRAS, 339, 897
Trager S. C., Worthey G., Faber S. M., Burstein D., González J. J., 1998, ApJS, 116, 1
Trager S. C., Faber S. M., Worthey G., González J. J., 2000, AJ, 119, 1645
Tripicco M. J., Bell R. A., 1995, AJ, 110, 3035
Valdes F., Gupta R., Rose J. A., Singh H. P., Bell D. J., 2004, ApJS, 152, 251
Vazdekis A., 1999, ApJ, 513, 224 (V99)
Vazdekis A., Arimoto N., 1999, ApJ, 525, 144
Vazdekis A., Casuso E., Peletier R. F., Beckman J. E., 1996, ApJS, 106, 307
Vazdekis A., Salaris M., Arimoto N., Rose J. A., 2001a, ApJ, 549, 274
Vazdekis A., Kuntschner H., Davies R. L., Arimoto N., Nakamura O., Peletier R., 2001b, ApJ, 551, L127
Vazdekis A., Peletier R. F., Beckman J. E., Casuso E., 1997, ApJS, 111, 203
Vazdekis A., Cenarro A. J., Gorgas J., Cardiel N., Peletier R. F., 2003, MNRAS, 340, 1317 (V03)
Wild V., Walcher C. J., Johansson P. H., Tresse L., Charlot S., Pollo A., Le Fèvre O., de Ravel L., 2009, MNRAS, 395, 144
Worthey G., 1994, ApJS, 95, 107
Worthey G., Ottaviani D. L., 1997, ApJS, 111, 377
Worthey G., Lee H.-C., 2006, preprint (astro-ph/0604590)
Worthey G., Faber S. M., González J. J., 1992, ApJ, 398, 69
Worthey G., Faber S. M., Gonzalez J. J., Burstein D., 1994, ApJS, 94, 687
Yamada Y., Arimoto N., Vazdekis A., Peletier R., 2006, ApJ, 637, 200
Zwitter T., Castelli F., Munari U., 2004, A&A, 417, 1055

APPENDIX A: TRANSFORMATIONS FROM THE LICK/IDS SYSTEM TO THE NEW LINE INDEX SYSTEM

In this appendix, we provide the required transformations that make it possible to convert Lick/IDS index measurements to the new system proposed here. For this purpose, we have compared the index measurements of the 218 MILES stars in common with the Lick library. The indices were measured once the MILES stellar spectra were broadened to 5.0, 8.4 and 14.0 Å to obtain the conversions corresponding to LIS-5.0 Å, LIS-8.4 Å and LIS-14.0 Å, respectively. To calculate these conversions, we fitted third-order polynomials in all cases. These polynomials are defined as follows:

$$I_{\rm LIS} = a_0 + a_1 I_{\rm Lick/IDS} + a_2 I^2_{\rm Lick/IDS} + a_3 I^3_{\rm Lick/IDS}, \quad \text{(A1)}$$

where $I_{\rm LIS}$ and $I_{\rm Lick/IDS}$ represent the index values in the LIS (at either of the three resolutions) and Lick/IDS system, respectively. Fig. A1 shows the results of the comparison between the indices of the Lick/IDS library and of MILES at FWHM = 5 Å resolution. Similarly, Figs A2 and A3 show the comparison of the indices

Table A1. Polynomials to transform from the Lick/IDS system to the new system defined here for GC (LIS-5.0 Å) (see equation A1).

Index	a_0	a_1	a_2	a_3
CN_1	0.018	0.941	−0.137	0.352
CN_2	0.027	0.955	−0.059	0.106
Ca4227	0.253	0.738	0.177	−0.018
G4300	0.709	0.944	0.029	−0.006
Fe4383	0.211	0.923	−0.005	0.001
Ca4455	0.035	0.602	0.250	−0.032
Fe4531	0.304	1.092	−0.046	0.002
C4668	0.642	0.831	0.017	
Hβ	0.116	1.001	−0.003	0.001
Fe5015	−0.154	1.162	−0.025	
Mg_1	−0.001	0.886	0.146	0.140
Mg_2	−0.004	0.924	0.013	−0.028
Mgb	0.116	0.950	0.009	−0.001
Fe5270	0.256	0.705	0.122	−0.013
Fe5335	0.259	0.805	0.141	−0.019
Fe5406	0.289	0.629	0.266	−0.047
Fe5709	0.006	1.045	−0.052	0.016
Fe5782	0.119	0.467	0.693	−0.213
Na5895	−0.074	0.921	0.023	−0.001
TiO_1	−0.004	0.773	0.723	−0.826
TiO_2	0.001	0.924	0.116	−0.132
Hδ_A	−0.369	1.012	1.012	
Hγ_A	−0.151	0.974	0.001	
Hδ_F	0.028	0.970	0.037	−0.003
Hγ_F	−0.174	1.050	0.013	−0.002

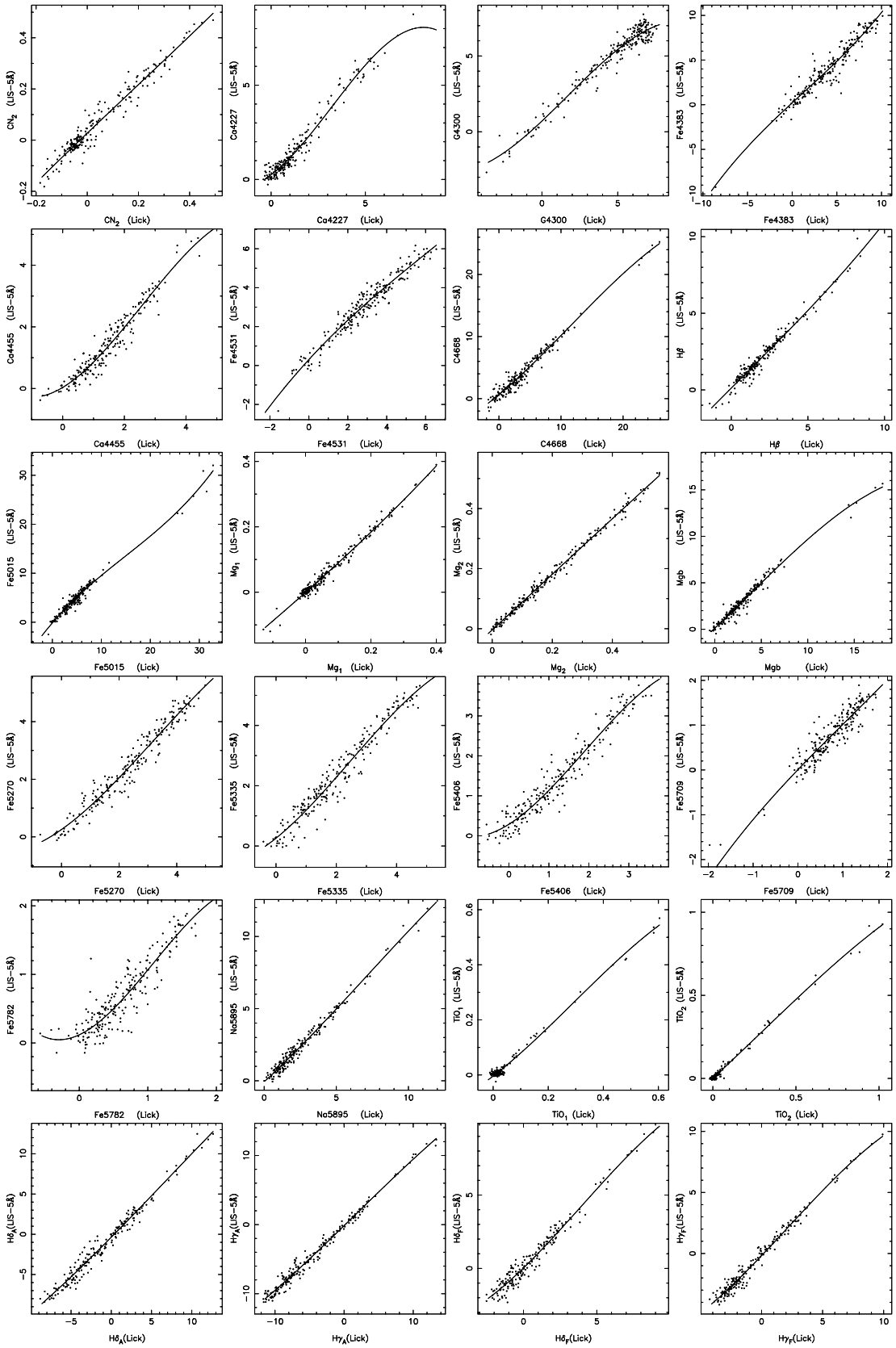

Figure A1. Comparison of the Lick/IDS indices of the Lick/IDS library and those in MILES broadened to a constant resolution FWHM = 5 Å. Solid lines show the transformation from one system to the other.

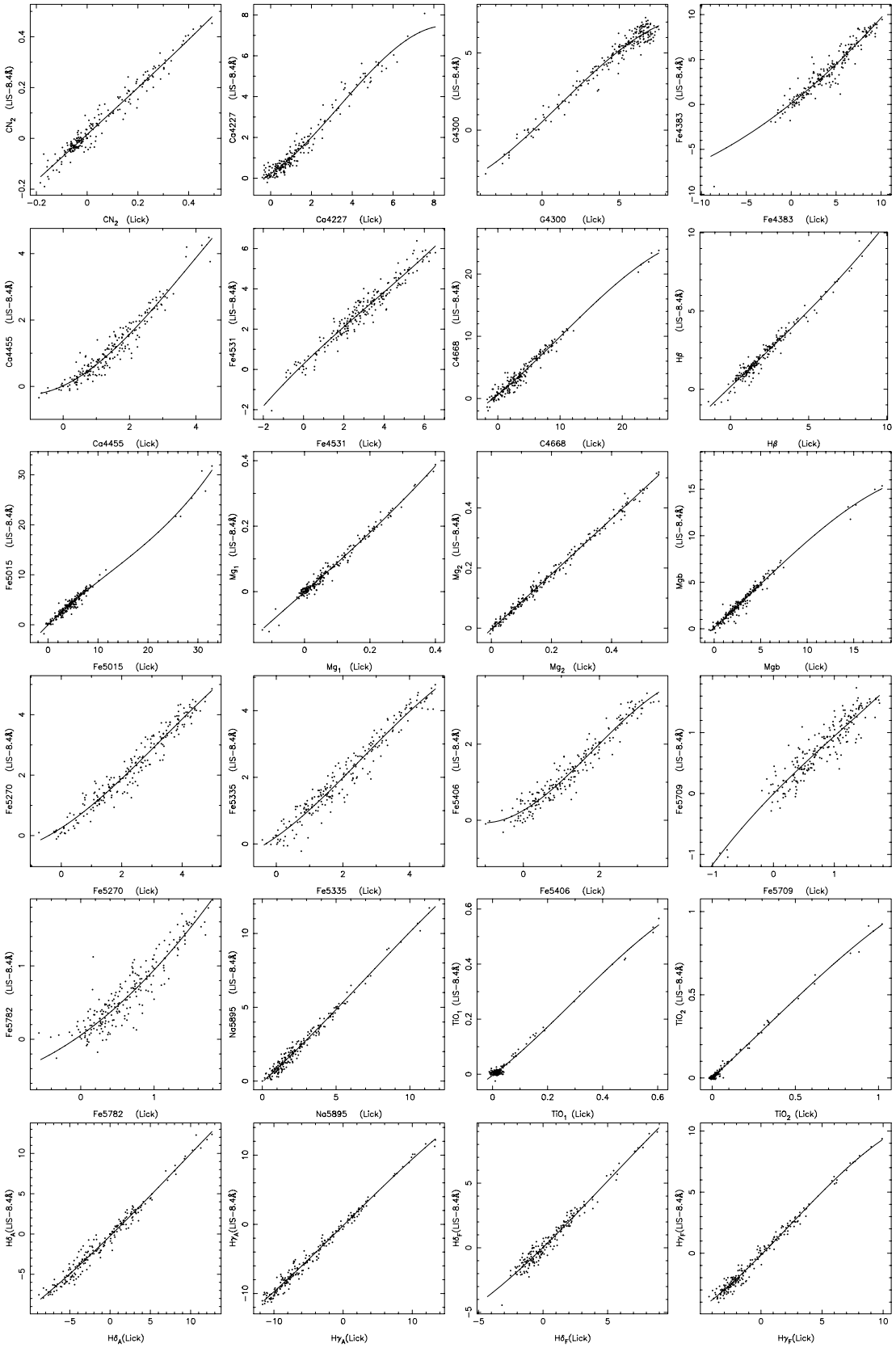

Figure A2. Comparison between the Lick/IDS indices of the Lick library and those measured on the stars in common with the MILES library broadened to FWHM = 8.4 Å. Solid lines represent the transformation from one system to the other (see Table A2).

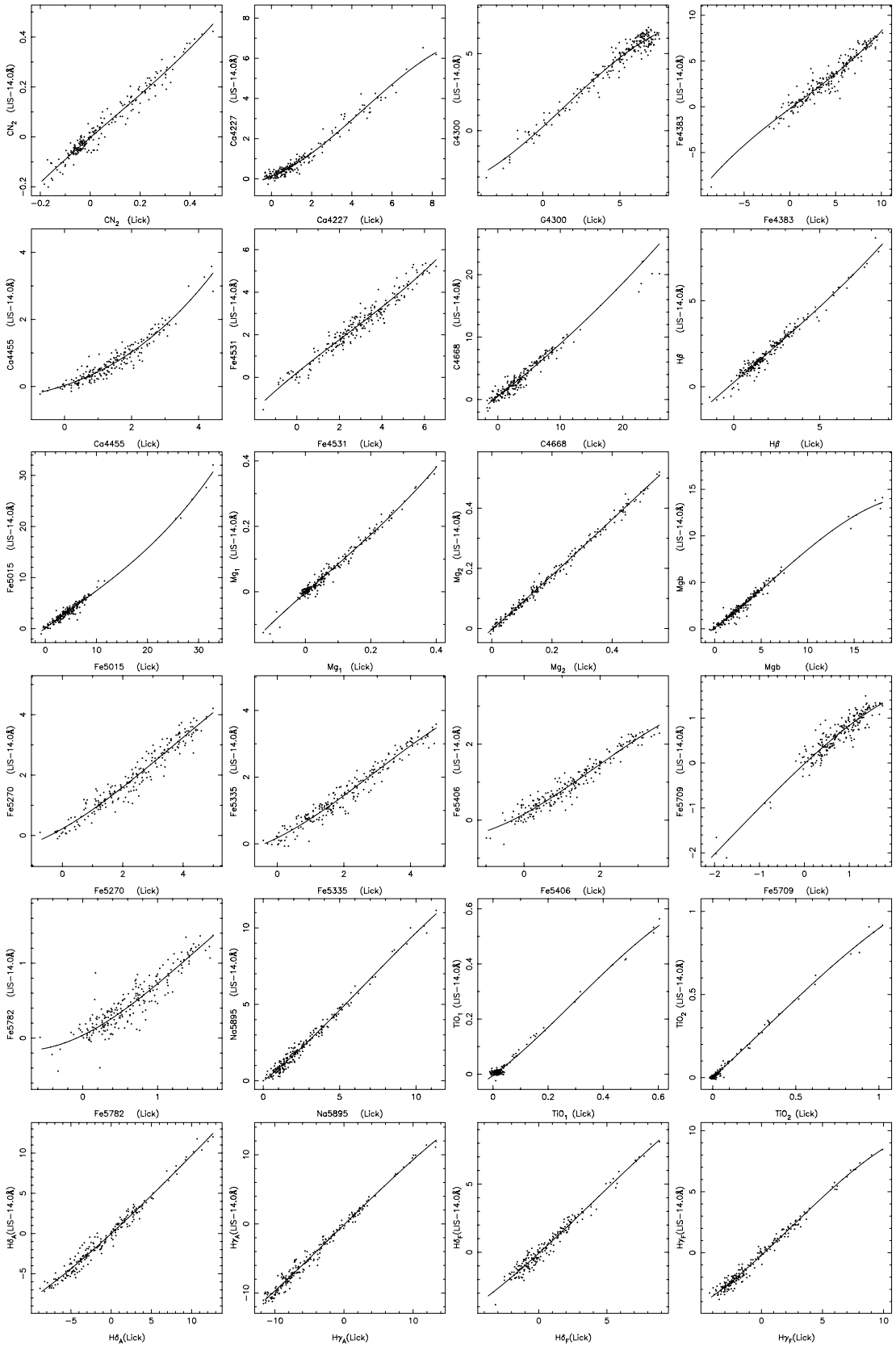

Figure A3. Comparison between the Lick/IDS indices of the Lick library and those measured on the stars in common with the MILES library broadened to FWHM = 14 Å. Solid lines represent the transformation from one system to the other (see Table A3).

Table A2. Polynomials to transform from the Lick/IDS system to the new system defined here for dwarf and intermediate-mass galaxies (LIS-8.4 Å).

	a_0	a_1	a_2	a_3
CN_1	0.011	0.913	−0.119	0.400
CN_2	0.016	0.911	0.025	0.076
Ca4227	0.217	0.668	0.140	−0.014
G4300	0.541	0.540	0.015	−0.004
Fe4383	0.106	0.796	0.015	
Ca4455	0.021	0.466	0.187	−0.016
Fe4531	0.267	0.972	−0.032	0.003
C4668	0.616	0.819	0.017	
Hβ	0.159	0.953	−0.002	0.001
Fe5015	−0.037	0.994	−0.018	
Mg_1	−0.001	0.884	0.056	0.358
Mg_2	−0.004	0.906	0.054	−0.051
Mgb	0.116	0.912	0.009	−0.001
Fe5270	0.253	0.649	0.104	−0.010
Fe5335	0.214	0.708	0.120	−0.015
Fe5406	0.257	0.587	0.225	−0.040
Fe5709	−0.005	1.024	−0.108	0.030
Fe5782	0.055	0.707	0.182	
Na5895	−0.057	0.887	0.025	−0.001
TiO_1	−0.004	0.766	0.736	−0.841
TiO_2	0.001	0.919	0.128	−0.142
Hδ_A	−0.246	0.977	0.006	
Hγ_A	−0.175	0.986		
Hδ_F	0.027	0.973	0.016	−0.001
Hγ_F	−0.149	1.010	0.015	−0.002

Table A3. Polynomials to transform from the Lick/IDS system to the new system defined here for massive galaxies (LIS-14.0 Å).

	a_0	a_1	a_2	a_3
CN_1	0.005	0.875	−0.091	0.402
CN_2	−0.002	0.863	−0.110	0.477
Ca4227	0.134	0.380	0.113	−0.008
G4300	0.251	0.910	0.019	−0.004
Fe4383	−0.203	0.749	−0.004	0.001
Ca4455	0.031	0.331	0.073	0.005
Fe4531	0.211	0.814	−0.025	0.004
C4668	0.500	0.779	0.006	
Hβ	0.257	0.861	−0.003	0.001
Fe5015	0.123	0.738	−0.004	
Mg_1	−0.003	0.885	−0.164	0.856
Mg_2	−0.003	0.874	0.154	−0.134
Mgb	0.112	0.738	0.022	−0.001
Fe5270	0.224	0.565	0.076	−0.007
Fe5335	0.178	0.496	0.090	−0.010
Fe5406	0.160	0.547	0.084	−0.015
Fe5709	−0.018	0.929	−0.064	−0.013
Fe5782	0.038	0.490	0.254	−0.056
Na5895	−0.022	0.801	0.034	−0.002
TiO_1	−0.004	0.749	0.798	−0.902
TiO_2	0.000	0.909	0.144	−0.155
Hδ_A	−0.017	0.914	0.008	
Hγ_A	−0.126	0.971		
Hδ_F	−0.074	0.909	0.013	−0.001
Hγ_F	−0.199	0.925	0.014	−0.002

of the Lick/IDS stars and of the MILES stars broadened to FWHM = 8.4 14 Å, respectively. The coefficients of these polynomials, which convert the Lick/IDS indices to the LIS-5.0 Å, LIS-8.4 Å and LIS-14.0 Å, are given in Tables A1–A3, respectively.

SUPPORTING INFORMATION

Additional Supporting Information may be found in the online version of this article:

Table 2. Lick indices measured in the LIS for GCs and galaxies from selected references.

This paper has been typeset from a TEX/LATEX file prepared by the author.